Ludwig-Maximillians-Universtät Müchen
Technische Universität Müchen
Max-Planck-Institut Für Quantumoptik

Variational theory of Angulons and their rotational spectroscopy

München 2022 Zhongda Zeng

Variational theory of Angulons and their rotational spectroscopy

Zhongda Zeng

Thesis submitted
within the Elite Master Program
Theoretical and Mathematical Physics
of Ludwig–Maximilians–Universität
München

Supervised by:
Prof. Dr. Richard Schmidt
Prof. Dr. Ignacio Cirac

München, submitted upon completion

Abstract

The study of isolated molecules in a superfluid matrix has attracted tremendous attention in recent decades thanks to advances in experimental techniques. The angulon, a quasiparticle formed by a quantum rotor immersed in a many-body bath, can effectively and efficiently characterize this rotating impurity problem.

We provide a comprehensive theoretical description of angulons, using a coherent state ansatz in the co-rotating frame. Employing a saddle point analysis and a time-dependent variational method, we calculate quasiparticle properties such as the effective rotational constants, the quasiparticle renormalization factor, and the quasiparticle spectral function. We compare the predictions of this ansatz to those of a single-excitation ansatz to gain a better understanding of the angulon in the intermediate-density regime. In the second part, we then discuss rotational spectroscopy, which focuses on the response of rotating molecules to a laser perturbation in the linear response regime. Importantly, we take into account initial-state interactions, which have been neglected in the prior research. Using a single-excitation ansatz to examine the angulon instability regime, we obtain consistent results with experiments, where the broadening of the spectral line is observed while phonon wings remain highly suppressed. Our findings confirm the validity of the single-excitation ansatz for describing excited states and suggest that a non-equilibrium initial state might recover the phonon wings in experiments.

Contents

List of Figures

Chapter 1

Introduction

Studying molecules in helium nanodroplets has attracted great interest in molecular physics and chemistry in recent decades [1, 2]. Here the nanodroplets act as a stable and efficient refrigerator, cooling molecules to an ultralow temperature, $\sim$ 0.37 Kelvin. They also provide a clean environment to manipulate and investigate molecules by performing for instance the spectroscopy and observing their chemical reactions [3–6]. While helium's superfluidity prevents the collisional and Doppler broadening of molecular spectral lines, the interaction between the molecule and helium causes a redshift and an anomalous broadening of spectral lines in rotational spectroscopy [7]. As a result, it is critical to understand how the molecule interacts with the droplet environment.

A molecule immersed in superfluid nanodroplets is an instance of quantum impurity problems that provide efficient descriptions to this intrinsic quantum many-body physics. The polaron problem is a well-known example. The idea was first proposed by Landau [8] and Pekar [9], and later developed by Fröhlich [10]. It describes a moving electron in a crystal environment. The electron dressed by phonons excited from the lattice forms a quasiparticle, the polaron. Likewise, the molecule-superfluid system can be theoretically described by an impurity with rotational degrees of freedom - a quantum rotor - embedded in a many-body bath. The rotor exchanges orbital angular momentum with bath, similar to polaron problems where the impurity exchanges momentum, but it is more challenging to solve due to the rotor's internal structure and non-Abelian $SO(3)$ algebra.

Several attempts have been made to investigate the rotor problems based on the first principle calculations with quantum Monte Carlo simulations [11–

13]. A microscopy theory has recently been proposed to effectively characterize such systems, in which the quantum rotor dressed by phonon excitations forms a quasiparticle known as the angulon [14–16]. With the good agreement with experiments, this theory provides a new theoretical understanding of the problem.

It characterizes, for example, the renormalization of rotational constants in a variety of molecules [17] using phenomenological approaches. Another example is the study of rotational spectroscopy based on a single-excitation ansatz [14]. The angulon picture offers a relatively simple approach to complex molecule physics, while experimental evidence backs up the validity of the picture [18].

Despite its elegance, the angulon model is still difficult to solve due to the infinite dimension of Hilbert space of phonons and the non-Abelian $SO(3)$ algebra of quantum rotor and previous variational theories are incomplete. On the one hand, they are unable to describe the renormalization of rotational constants in a general way. On the other hand, angulon theory predicts significant phonon wings, which emerge from the sharp spectral lines and dominate the spectrum in instability regimes. However, phonon wings are hardly seen in experiments.

The goal of this thesis is to resolve the two issues mentioned above. Concerning the first, we propose a coherent state ansatz in the co-rotating frame and conduct a variational study of angulons. This method provides a simple picture that can be used to access both static and dynamic properties. Remarkably, the ground state can be described by a macroscopic wavefunction that is a product state of a bosonic and anomalous spin coherent state. It further provides reasonable predictions for the renormalization of the rotational constant. Moreover, we study the quasiparticle spectrum, where an intermediate instability regime exists. Concerning the second challenge, we study the rotational spectroscopy of $L = 0 \to 1$ transition using the single-excitation ansatz within the linear response theory, in which the initial state is taken to be the angulon ground state rather than the vacuum state. We show that there exists an instability regime in the spectrum but no phonon wings which is consistent with experiments. This emphasizes the significant role of the molecule-bath initial-state interaction. We also consider the coherent state ansatz. However, regardless of density, it always predicts a shape spectral line, which implies the coherent state is insufficient to accurately describe excited states.

The thesis is structured as follows. In Chapter 2, the Fröhlich polaron

is introduced, which is one of the most well-known impurity models. We then go through two common methods, the perturbation theory and Lee-Low-Pines theory, which pave the way to the two methods we use to solve the angulon model. In Chapter 3, the angulon model is revisited and the single-excitation ansatz is briefly introduced. Beyond the prior studies, we derive the real-time evolution equations for the single-excitation ansatz. Afterward, in Chapter 4, we present the coherent state ansatz in the rotor's co-rotating frame. We use an iterative imaginary-time evolution and exact diagonalization method to examine the static properties, such as the renormalization of the rotational constant. In addition, real-time evolution is employed to study the quasiparticle spectrum. In Chapter 5, we investigate rotational spectroscopy in detail. We find that numerical predictions based on the single-excitation ansatz are compatible with experiments, exhibiting an instability regime but no phonon wings if one considers an equilibrium initial-state within linear response theory. Finally, the work is summarized and potential generalizations are discussed in Chapter 6.

Chapter 2

Paradigm of Quantum Impurity problems: Fröhlich Polarons

The concept of polaron originates from Landau [8] and Pekar [9] in studying moving electrons in a solid-state crystal. The electrons cause a vibration of atoms in the lattice, which generates a collective excitation, the phonon. The electron dressed by phonons forms a quasiparticle, known as a polaron. The polaron, which plays a key role in electron transport, is different from the bare electron in the effective mass and the response to external fields. But the polaron problem is usually hard to solve analytically and remains one of the most significant quantum many-body problems despite the long history of studies.

With the development of experimental techniques, such as ultracold quantum gases [19], polaron physics attracts tremendous attention again. Experimentalists are interested in continuous media, such as immersing the impurity in Bose or Fermi gases [20–25], in addition to studies of impurities in lattices [26–28]. The concept of polarons can help to understand the formation of few-body bound states [29, 30] and even Bose-Fermi mixtures [31, 32].

In this chapter, we will introduce the Fröhlich polaron based on Ref. [33, 34]. Two archetypes for exploring the impurity problem will be shown: perturbation theory and a variational approach. These will provide hints for solving the Angulon problem in the following chapters.

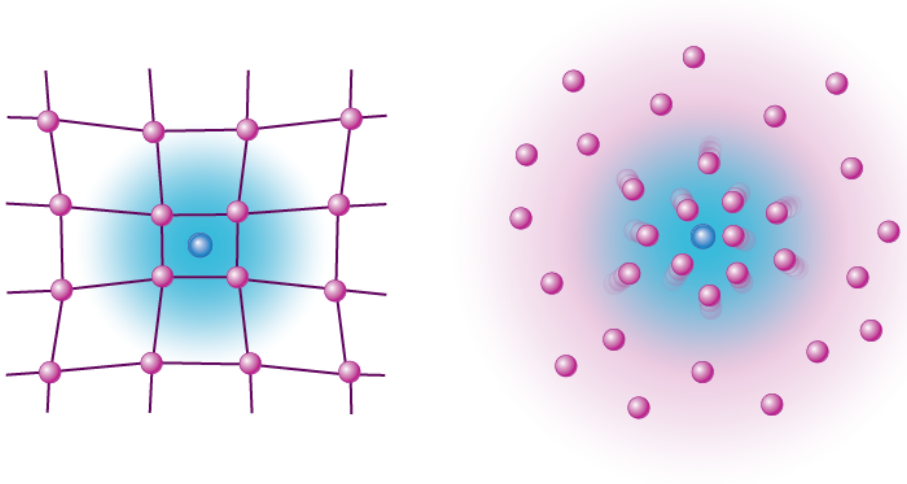

Figure 2.1: Schematic illustration of polaron, which is formed by a moving impurity immersed in a phonon bath. Adapted from Ref. [35].

2.1 Fröhlich polaron

The Fröhlich polaron is one of the most well-known polaron models [10]. It is also referred to as the large polaron. Because the size of the polaron is large in comparison to the lattice parameters of a solid, the medium can be treated continuously. The Hamiltonian is given by

$$\hat{H} = \frac{\hat{\boldsymbol{p}}^2}{2m} + \sum_{\boldsymbol{q}} \omega_{\mathrm{LO}} \hat{a}^\dagger_{\boldsymbol{q}} \hat{a}_{\boldsymbol{q}} + \sum_{\boldsymbol{q}} (V_q \hat{a}_{\boldsymbol{q}} e^{i\boldsymbol{q}\cdot\hat{\boldsymbol{r}}} + h.c.), \tag{2.1}$$

where $\hbar$ is set to be one and $\sum_{\boldsymbol{q}} = \int \frac{V d^3\boldsymbol{p}}{(2\pi)^3}$. $\hat{\boldsymbol{p}}$ and $\hat{\boldsymbol{r}}$ are the momentum and position operators of the moving impurity, respectively. The first term of Hamiltonian describes the kinetic energy of impurity. The second term describes the kinetic energy of excited phonons with the longitudinal optical dispersion ω_{LO}. The third term describes the electron-phonon interaction, where the interaction strength is given by

$$V_q = -i \frac{\omega_{\mathrm{LO}}}{q} \left(\frac{4\pi\alpha}{V}\right)^{1/2} \left(\frac{1}{2m\omega_{\mathrm{LO}}}\right)^{1/4}, \tag{2.2}$$

and the dimensionless coupling constant is given by

$$\alpha = \frac{e^2}{\hbar} \sqrt{\frac{m}{2\omega_{\mathrm{LO}}}} \left(\frac{1}{\varepsilon_\infty} - \frac{1}{\varepsilon_0}\right). \tag{2.3}$$

Here $q = |\boldsymbol{q}|$ and ε is the dielectric constant.

2.2 Perturbation theory

Fröhlich solved the model Eq. (2.1) using a weak-coupling perturbation theory which will be briefly introduced in this section.

The non-interacting Hamiltonian consists of kinetic energy terms for the impurity and phonons. Then the zero-order approximation state is given by

$$|\boldsymbol{k}; 0\rangle \equiv |\boldsymbol{k}\rangle \otimes |0\rangle, \tag{2.4}$$

which is a product state between the momentum eigenstate of impurity $|\boldsymbol{k}\rangle$ and the vacuum state for phonons $|0\rangle$. And the corresponding energy is given by

$$E_{\boldsymbol{k}}^{(0)} = \frac{k^2}{2m}. \tag{2.5}$$

Before considering the perturbation, we can rewrite the impurity's coordinate operators in the interaction Hamiltonian into momentum basis:

$$\begin{aligned} e^{i\boldsymbol{q}\cdot\hat{\boldsymbol{r}}} &= \sum_{\boldsymbol{x}} \sum_{\boldsymbol{p},\boldsymbol{k}} |\boldsymbol{p}\rangle\langle\boldsymbol{p}|\boldsymbol{x}\rangle e^{i\boldsymbol{q}\cdot\boldsymbol{x}} \langle\boldsymbol{x}|\boldsymbol{k}\rangle\langle\boldsymbol{k}| \\ &= \sum_{\boldsymbol{k}} |\boldsymbol{k}+\boldsymbol{q}\rangle\langle\boldsymbol{k}| \\ &= \sum_{\boldsymbol{k}} \hat{c}_{\boldsymbol{k}+\boldsymbol{q}}^{\dagger} \hat{c}_{\boldsymbol{k}}. \end{aligned} \tag{2.6}$$

Here we introduced the single-particle annihilation (creation) operators $\hat{c}_{\boldsymbol{k}}^{(\dagger)}$ for convenience, which only show up in pairs and describe the impurity-bath momentum transfer. Then the interaction term can be written as

$$\hat{H}_i = \sum_{\boldsymbol{q}} \sum_{\boldsymbol{k}} (V_q \hat{a}_{\boldsymbol{q}} \hat{c}_{\boldsymbol{k}+\boldsymbol{q}}^{\dagger} \hat{c}_{\boldsymbol{k}} + h.c.), \tag{2.7}$$

which explicitly exhibits the total momentum conservation between the impurity and phonons.

We then consider the second-order perturbation of the ground state, whose wavefunction is given by

$$\begin{aligned}|\psi\rangle =&|\boldsymbol{k};0\rangle + \sum_{\boldsymbol{q}} \frac{\langle \boldsymbol{k}-\boldsymbol{q};\boldsymbol{q}|\hat{H}_i|\boldsymbol{k};0\rangle}{\frac{k^2}{2m}-\frac{(\boldsymbol{k}-\boldsymbol{q})^2}{2m}-\omega_{\mathrm{LO}}}|\boldsymbol{k}-\boldsymbol{q};\boldsymbol{q}\rangle,\\ =&|\boldsymbol{k};0\rangle + \sum_{\boldsymbol{q}} \frac{V_q^*}{\frac{k^2}{2m}-\frac{(\boldsymbol{k}-\boldsymbol{q})^2}{2m}-\omega_{\mathrm{LO}}}|\boldsymbol{k}-\boldsymbol{q};\boldsymbol{q}\rangle,\end{aligned} \tag{2.8}$$

where $|\boldsymbol{k};\boldsymbol{q}\rangle = |\boldsymbol{k}\rangle \otimes |\boldsymbol{q}\rangle$ is the one-phonon excitation basis since the interaction only annihilates or excites one phonon and the transition matrix is given by

$$\begin{aligned}&\langle \boldsymbol{k}-\boldsymbol{q};\boldsymbol{q}|\hat{H}_i|\boldsymbol{k};0\rangle\\ =&\langle \boldsymbol{k}-\boldsymbol{q};\boldsymbol{q}|\sum_{\boldsymbol{q}}\sum_{\boldsymbol{k}}(V_q\hat{a}_{\boldsymbol{q}}\hat{c}^\dagger_{\boldsymbol{k}+\boldsymbol{q}}\hat{c}_{\boldsymbol{k}}+h.c.)|\boldsymbol{k};0\rangle\\ =&V_q^*.\end{aligned} \tag{2.9}$$

The perturbative energy is given by

$$\begin{aligned}E_{\boldsymbol{k}} =&\frac{k^2}{2m}+\sum_{\boldsymbol{q}}\frac{|\langle \boldsymbol{k}-\boldsymbol{q};\boldsymbol{q}|\hat{H}_i|\boldsymbol{k};0\rangle|^2}{\frac{k^2}{2m}-\frac{(\boldsymbol{k}-\boldsymbol{q})^2}{2m}-\omega_{\mathrm{LO}}}\\ =&\frac{k^2}{2m}+\sum_{\boldsymbol{q}}\frac{|V_q|^2}{\frac{k^2}{2m}-\frac{(\boldsymbol{k}-\boldsymbol{q})^2}{2m}-\omega_{\mathrm{LO}}}\\ =&\frac{k^2}{2m}+2m\omega_{\mathrm{LO}}^2(\frac{4\pi\alpha}{V})(\frac{1}{2m\omega_{\mathrm{LO}}})^{1/2}\sum_{\boldsymbol{q}}\frac{1}{q^2}\frac{1}{2\boldsymbol{k}\cdot\boldsymbol{q}-q^2-2m\omega_{\mathrm{LO}}}\\ \approx&-\alpha\omega_{\mathrm{LO}}+\frac{k^2}{2m}(1-\frac{\alpha}{6}).\end{aligned} \tag{2.10}$$

The energy of the quasiparticle can be written as $E_{\boldsymbol{k}} \approx E_0 + \frac{k^2}{2m^*}$, which defines the effective mass. By comparing the two formulas, one can obtain the effective mass

$$m^* = \frac{m}{1-\alpha/6} \approx m(1+\frac{\alpha}{6}). \tag{2.11}$$

Here $\alpha > 0$ indicates that the polaron is heavier than the bare electron, which means the dressing by the phonon cloud reduces the mobility of electron.

It is worth mentioning that the perturbation wavefunction can be generalized to a variational ansatz. One can propose a single-excitation trial wavefuntion, which is given by

$$|\psi\rangle = \phi_0|\boldsymbol{k};0\rangle + \sum_{\boldsymbol{q}} \phi_{\boldsymbol{q}}|\boldsymbol{k}-\boldsymbol{q};\boldsymbol{q}\rangle, \tag{2.12}$$

which is similar to the so-called Chevy ansatz [36]. A similar result to the perturbation theory can be obtained by minimizing the variational energy. The variational method has two benefits: the self-consistent normalization condition improves the accuracy of the variational study [16], and it is easy to extend to the study of real-time evolution.

2.3 Variational method

The variational method is an approach commonly used for impurity problems. Even though not providing exact solutions, it gives an upper bound estimate for the ground-state energy; and if the trial wavefunction is good enough, one can gain deep insight into the physics, such as the famous Laughlin wavefunctions [37]. Understanding the way that the impurity and bath couple together is the main challenge for guessing the trial wavefunction. The simplest way is the exchange of momentum up to the single-excitation discussed above. In this section, we will introduce the coherent state ansatz in the co-moving frame of the impurity, in which the Lee-Low-Pines transformation is employed to entangle the impurity and bath.

2.3.1 Lee, Low and Pines (LLP) Transformation

Before discussing the transformation, we first introduce the total momentum operator:

$$\hat{\boldsymbol{P}} = \hat{\boldsymbol{p}} + \sum_{\boldsymbol{q}} \boldsymbol{q}\hat{a}^\dagger_{\boldsymbol{q}}\hat{a}_{\boldsymbol{q}}. \tag{2.13}$$

One can easily check that it commutes with the Hamiltonian:

$$[\hat{\boldsymbol{P}}, \hat{H}], \tag{2.14}$$

which implies the total momentum is conserved. This implies that we can further introduce a canonical transformation to reduce the degrees of freedom

of the system. This is the so-called Lee, Low and Pines (LLP) transformation [38]:

$$\hat{U}_{\mathrm{LLP}} = e^{-i\hat{\boldsymbol{r}}\cdot\sum_{\boldsymbol{q}} \boldsymbol{q}\hat{a}^{\dagger}_{\boldsymbol{q}}\hat{a}_{\boldsymbol{q}}}, \tag{2.15}$$

which is generated by the momentum of phonons and is a translational transformation to the co-moving frame of the electron.

Here we lists some typical transformation of operators:

$$\begin{aligned}
&\hat{U}^{\dagger}_{\mathrm{LLP}}\hat{a}_{\boldsymbol{q}}\hat{U}_{\mathrm{LLP}} = \hat{a}_{\boldsymbol{q}}e^{-i\hat{\boldsymbol{r}}\cdot\boldsymbol{q}};\\
&\hat{U}^{\dagger}_{\mathrm{LLP}}\hat{\boldsymbol{p}}\hat{U}_{\mathrm{LLP}} = \hat{\boldsymbol{p}} - \sum_{\boldsymbol{q}} \boldsymbol{q}\hat{a}^{\dagger}_{\boldsymbol{q}}\hat{a}_{\boldsymbol{q}};\\
&\hat{U}^{\dagger}_{\mathrm{LLP}}\hat{\boldsymbol{P}}\hat{U}_{\mathrm{LLP}} = \hat{\boldsymbol{p}}.
\end{aligned} \tag{2.16}$$

The last equation indicates that the impurity momentum operator in the transferred frame represents the total momentum of the system in the original frame. The Hamiltonian in the co-moving frame reads:

$$\begin{aligned}
\hat{\mathcal{H}} =& \hat{U}^{\dagger}_{\mathrm{LLP}}\hat{H}\hat{U}_{\mathrm{LLP}}\\
=& \frac{1}{2m}(\hat{\boldsymbol{p}} - \sum_{\boldsymbol{q}} \boldsymbol{q}\hat{a}^{\dagger}_{\boldsymbol{q}}\hat{a}_{\boldsymbol{q}})^2 + \sum_{\boldsymbol{q}} \omega_{\mathrm{LO}}\hat{a}^{\dagger}_{\boldsymbol{q}}\hat{a}_{\boldsymbol{q}} + \sum_{q}(V_q\hat{a}_{\boldsymbol{q}} + h.c.).
\end{aligned} \tag{2.17}$$

The interaction term dose not contain impurity coordinates, and it commutes with the total momentum operator, $[\hat{\boldsymbol{p}}, \hat{\mathcal{H}}]$. Hence we can replace the momentum operators by a c-number $\hat{\boldsymbol{p}} \to \boldsymbol{p}$, and solve the model in each total momentum sector. The impurity is now fully decoupled and the model is purely bosonic. In this case, many methods can be employed, and as an example, we will next show a coherent state ansatz.

2.3.2 Coherent state ansatz

We first consider the ground state, for which we set $\boldsymbol{p} = 0$. The Hamiltonian then reduces to

$$\begin{aligned}\hat{\mathcal{H}}(0) =&\frac{1}{2m}(\sum_{\boldsymbol{q}} \boldsymbol{q}\hat{a}^\dagger_{\boldsymbol{q}}\hat{a}_{\boldsymbol{q}})^2 + \sum_{\boldsymbol{q}} \omega_{\mathrm{LO}}\hat{a}^\dagger_{\boldsymbol{q}}\hat{a}_{\boldsymbol{q}} + \sum_{q}(V_q\hat{a}_{\boldsymbol{q}} + h.c.)\\ =&\sum_{\boldsymbol{q},\boldsymbol{q}'} \frac{\boldsymbol{q}\cdot\boldsymbol{q}'}{2m}\hat{a}^\dagger_{\boldsymbol{q}}\hat{a}^\dagger_{\boldsymbol{q}'}\hat{a}_{\boldsymbol{q}}\hat{a}_{\boldsymbol{q}'} + \sum_{\boldsymbol{q}}(\omega_{\mathrm{LO}} + \frac{q^2}{2m})\hat{a}^\dagger_{\boldsymbol{q}}\hat{a}_{\boldsymbol{q}} + \sum_{\boldsymbol{q}}(V_q\hat{a}_{\boldsymbol{q}} + h.c.)\\ \approx&\sum_{\boldsymbol{q}}(\omega_{\mathrm{LO}} + \frac{q^2}{2m})\hat{a}^\dagger_{\boldsymbol{q}}\hat{a}_{\boldsymbol{q}} + \sum_{\boldsymbol{q}}(V_q\hat{a}_{\boldsymbol{q}} + h.c.),\end{aligned} \tag{2.18}$$

where the quartic term of phonon interaction is ignored in the last line since the ground state is assumed to be isotropic.

This Hamiltonian can be diagonalized by a displacement transformation:

$$\hat{U}_{\mathrm{c}} = \exp(\sum_{\boldsymbol{q}} \hat{a}^\dagger_{\boldsymbol{q}}\beta_{\boldsymbol{q}} - \beta^*_{\boldsymbol{q}}\hat{a}_{\boldsymbol{q}}), \tag{2.19}$$

where the displacement is given by

$$\beta_{\boldsymbol{q}} = -\frac{V^*_q}{\omega_{\mathrm{LO}} + \frac{q^2}{2m}}. \tag{2.20}$$

And the Hamiltonian after transformation is given by

$$\begin{aligned}&\hat{U}^\dagger_{\mathrm{c}}\hat{\mathcal{H}}(0)\hat{U}_{\mathrm{c}}\\ =&\sum_{\boldsymbol{q}}(\omega_{\mathrm{LO}} + \frac{q^2}{2m})(\hat{a}^\dagger_{\boldsymbol{q}} + \beta^*_{\boldsymbol{q}})(\hat{a}_{\boldsymbol{q}} + \beta_{\boldsymbol{q}}) + \sum_{q}(V_q(\hat{a}_{\boldsymbol{q}} + \beta_{\boldsymbol{q}}) + h.c.)\\ =&(\omega_{\mathrm{LO}} + \frac{q^2}{2m})\hat{a}^\dagger_{\boldsymbol{q}}\hat{a}_{\boldsymbol{q}} - \sum_{\boldsymbol{q}} \frac{|V_q|^2}{\omega_{\mathrm{LO}} + \frac{q^2}{2m}}.\end{aligned} \tag{2.21}$$

Explicitly, the ground state is the vacuum state for phonons in the transferred frame, and in the original frame the overall ground state is given by

$$|\psi_0\rangle = \hat{U}_{\mathrm{LLP}}(|0\rangle_{\mathrm{m}} \otimes \hat{U}_{\mathrm{c}}|0\rangle_b), \tag{2.22}$$

where $|0\rangle_b$ represents the vacuum state for phonons and $|0\rangle_i$ represents zero total momentum state such that $\hat{\boldsymbol{p}}|0\rangle_{\rm m}=0$ and $\hat{\boldsymbol{P}}|\psi_0\rangle=0$. The corresponding ground state energy can be written as

$$\begin{aligned} E(0) =& -\sum_{\boldsymbol{q}} \frac{|V_q|^2}{\omega_{\rm LO}+\frac{q^2}{2m}} \\ =& -\sum_{\boldsymbol{q}} \frac{(\frac{\omega_{\rm LO}}{q})^2 \frac{4\pi\alpha}{V} (\frac{1}{2m\omega_{\rm LO}})^{1/2}}{\hbar\omega_{\rm LO}+\frac{q^2}{2m}} \\ =& -\alpha\omega_{\rm LO}\frac{2}{\pi}\int_0^\infty \frac{d\xi}{1+\xi^2} \\ =& -\alpha\omega_{\rm LO}, \end{aligned} \tag{2.23}$$

where $\sum_{\boldsymbol{q}} \to V\int_0^\infty q^2dq/(2\pi^2)$. The ground-state energy is consistent with the perturbation theory result.

Our next goal is to study the effective mass of the polaron, and we thus consider a general $\boldsymbol{p}$. It is natural to generalize the ground-state wavefunction into a variational ansatz:

$$|\psi_{\boldsymbol{p}}\rangle = \hat{U}_{\rm LLP}(|\boldsymbol{p}\rangle_{\rm m}\otimes\hat{U}_{\rm c}|0\rangle_b), \tag{2.24}$$

where the parameters $\beta_{\boldsymbol{q}}^{(*)}$ in the displacement transformation $\hat{U}_{\rm c}$ are treated as variationally, and $|\boldsymbol{p}\rangle_{\rm m}$ represent the total momentum state.

For the general case, we can first expand the Hamiltonian in normal order:

$$\begin{aligned} \hat{\mathcal{H}}(\boldsymbol{p}) =& \frac{1}{2m}(\boldsymbol{p}-\sum_{\boldsymbol{q}}\boldsymbol{q}\hat{a}_{\boldsymbol{q}}^\dagger\hat{a}_{\boldsymbol{q}})^2+\sum_{\boldsymbol{q}}\omega_{\rm LO}\hat{a}_{\boldsymbol{q}}^\dagger\hat{a}_{\boldsymbol{q}}+\sum_q(V_q\hat{a}_{\boldsymbol{q}}+h.c.) \\ =& \frac{p^2}{2m}+\sum_{\boldsymbol{q}}(V_q\hat{a}_{\boldsymbol{q}}+h.c.) \\ &+\sum_{\boldsymbol{q}}(\omega_{\rm LO}-\frac{1}{m}\boldsymbol{p}\cdot\boldsymbol{q}+\frac{q^2}{2m})\hat{a}_{\boldsymbol{q}}^\dagger\hat{a}_{\boldsymbol{q}}+\sum_{\boldsymbol{q},\boldsymbol{q}'}\frac{\boldsymbol{q}\cdot\boldsymbol{q}'}{2m}\hat{a}_{\boldsymbol{q}}^\dagger\hat{a}_{\boldsymbol{q}'}^\dagger\hat{a}_{\boldsymbol{q}}\hat{a}_{\boldsymbol{q}'}, \end{aligned} \tag{2.25}$$

And we can easily write down the variational energy for the coherent state

ansatz:

$$\begin{aligned} E_{\boldsymbol{p}} =& \langle \psi_{\boldsymbol{p}} | \hat{H} | \psi_{\boldsymbol{p}} \rangle \\ =& \frac{p^2}{2m} + \sum_{\boldsymbol{q}} (V_q \beta_{\boldsymbol{q}} + h.c.) \\ &+ \sum_{\boldsymbol{q}} (\omega_{\mathrm{LO}} - \frac{\boldsymbol{p} \cdot \boldsymbol{q}}{m} + \frac{q^2}{2m}) |\beta_{\boldsymbol{q}}|^2 + \frac{1}{2m} (\sum_{\boldsymbol{q}} \boldsymbol{q} |\beta_{\boldsymbol{q}}|^2)^2. \end{aligned} \tag{2.26}$$

To minimize the variational energy, we employ the variational principle:

$$\frac{\partial E_{\boldsymbol{p}}}{\partial \beta_{\boldsymbol{q}}} = \frac{\partial E_{\boldsymbol{p}}}{\partial \beta^*_{\boldsymbol{q}}} = 0. \tag{2.27}$$

This gives rise to self-consistent equations. Here we skip the lengthy derivation and point out the results directly. The energy for general $\boldsymbol{p}$ is given by:

$$E_p = -\alpha \omega_{\mathrm{LO}} + \frac{p^2}{2m[1 + \alpha/6)]}, \tag{2.28}$$

and the effective mass:

$$m^* = m(1 + \frac{\alpha}{6}), \tag{2.29}$$

which is again consistent with the perturbation theory.

However, despite the consistency, the coherent state ansatz is more general since it does not require the interaction strength $\alpha \ll 1$. And physically speaking the coherent state includes an infinite number of phonon excitation terms, and is the exact solution in the large mass limit.

142. Paradigm of Quantum Impurity problems: Fröhlich Polarons

Chapter 3

Quantum Rotor in Bosonic Bath: Angulon

Even for a single molecule, a complete theoretical description is difficult because it has many degrees of freedom [39, 40]: the translation of the center of mass, the rotation and vibration between nuclei, and the motion of electrons. And the many-body bath must be considered when studying an isolated molecule in a superfluid. As a result, an effective comprehensible model is necessary.

Fortunately, one can only consider the molecule's rotational degrees of freedom when focusing on rotational spectroscopy. And the quantum rigid rotor is a reasonable approximation for it. For such a rotor-bath model, many first-principle calculations have been performed [11–13]. To avoid the expensive calculations, the Bogoliubov phonon can be used to approximate the superfluid bath. Similar to the polaron, a quantum rotor dressed by the phonon cloud forms a quasiparticle, angulon. The angulon model, which can be solved variationally, provides an effective and efficient description of experiments. For example, one can describe the effective rotational constants by phenomenological theories [17], and explain the anomalous broadening of spectral lines by variational theories [18].

In this chapter, we will introduce the setup of the Angulon Hamiltonian first, followed by a variational study based on a single-excitation ansatz [14, 16]. Furthermore, we will derive the equations of motion for the single-excitation ansatz, which is more convenient for numerical calculations and will be useful in calculating the rotational spectroscopy.

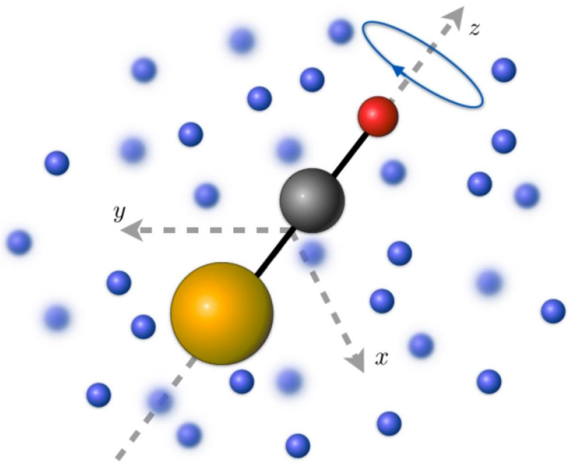

Figure 3.1: Schematic illustration of angulon, which is formed by a quantum rigid rotor dressed by phonons. Adapted from Ref. [41].

3.1 Angulon model

We consider a linear molecule in a superfluid nanodroplet at zero temperature. The system can be described by a quantum rotor dressed by the Bogoliubov phonons excited from a weakly interacting bosonic bath. The Hamiltonian is given by [14]:

$$\hat{H} = B\hat{\boldsymbol{J}}^2 + \sum_{k\lambda\mu} \omega_k \hat{b}^\dagger_{k\lambda\mu}\hat{b}_{k\lambda\mu} + \sum_{k\lambda\mu} U_\lambda(k)[Y^*_{\lambda\mu}(\hat{\theta},\hat{\phi})\hat{b}^\dagger_{k\lambda\mu} + Y_{\lambda\mu}(\hat{\theta},\hat{\phi})\hat{b}_{k\lambda\mu}], \quad (3.1)$$

where $\hbar \equiv 1$ and $\sum_k \equiv \int dk$. The Hamiltonian consists of three terms. The first term represents the rotational kinetic energy of a rotor where B is the rotational constant, and $\hat{\boldsymbol{J}}$ are the angular momentum operators in the lab frame. The second term represents the kinetic energy of excited phonons. The bosonic operators, $\hat{b}^{(\dagger)}_{k\lambda\mu}$, are in angular momentum representation,

$$\hat{b}^\dagger_{k\lambda\mu} = \frac{k}{(2\pi)^{3/2}} \int \sin\theta_k d\theta_k d\phi_k i^{-\lambda} Y_{\lambda\mu}(\theta_k,\phi_k)\hat{b}^\dagger_{\boldsymbol{k}}, \quad (3.2)$$

where $k = |\boldsymbol{k}|$ indicates the momentum amplitude; λ and μ label the angular momentum quantum number and its projection to z axis in the lab frame. More details are shown in appendix. Here we consider a superfluid bath with

dispersion relation $\omega_k = \sqrt{\epsilon_k(\epsilon_k + 2g_{\rm bb}n)}$, where $g_{bb} = 4\pi a_{\rm bb}/m$, and we set $a_{\rm bb} = 3.3(mB)^{-1/2}$ for the scattering length of ^{4}He. The last term represents the interaction between the rotor and the phonon bath, which couples the angles of the rotor, $\hat{\theta}$ and $\hat{\phi}$, with the phonon fluctuation; $j_\lambda(kr)$ is the spherical Bessel function and $Y_{\lambda\mu}(\hat{\theta}, \hat{\phi})$ is the spherical harmonics. The interaction strength is given by $U_\lambda(k) = u_\lambda[\frac{8nk^2\epsilon_k}{\omega_k(2\lambda+1)}]^{1/2} \int drr^2 f_\lambda(r) j_\lambda(kr)$, where we consider Gaussian form factors, $f_\lambda(r) = (2\pi)^{-3/2} e^{-r^2/(2r_\lambda^2)}$, and the interaction amplitudes and ranges are $u_0 = 1.75u_1 = 218B$ and $r_0 = r_1 = 1.5(mB)^{-1/2}$. Apart from the rotor, we introduce the angular momentum of the phonon bath $\hat{\Lambda}^\alpha = \sum_{k\lambda\mu\nu} \hat{b}^\dagger_{k\lambda\mu} \sigma^{\lambda,\alpha}_{\mu\nu} \hat{b}_{k\lambda\nu}$, and further introduce the total angular momentum $\hat{\boldsymbol{L}} = \hat{\boldsymbol{J}} + \hat{\boldsymbol{\Lambda}}$. It is easy to check that the Angulon Hamiltonian commutes with $\hat{\boldsymbol{L}}$ and its square $\hat{\boldsymbol{L}}^2$, which indicates that the eigenstates are labeled by two quantum numbers, L and M, correspondingly

$$\begin{aligned} \hat{L}^z|L, M\rangle &= M|L, M\rangle, \\ \hat{\boldsymbol{L}}^2|L, M\rangle &= L(L+1)|L, M\rangle. \end{aligned} \tag{3.3}$$

The Angulon Hamiltonian is similar to Fröhlich polaron:

Fröhlich polaron	Angulon
Momentum: $\hat{\boldsymbol{p}}$	Angular Momentum: $\hat{\boldsymbol{J}}$
Coordinate: $\hat{\boldsymbol{r}}$	Polar Angle: $\hat{\theta}$, $\hat{\phi}$
Mass: m	Rotational Constant: B
$e^{i\boldsymbol{k}\cdot\hat{\boldsymbol{r}}}$	$Y_{\lambda\mu}(\hat{\theta}, \hat{\phi})$
$[\hat{H}, \hat{\boldsymbol{P}}] = 0$	$[\hat{H}, \hat{\boldsymbol{L}}^2] = [\hat{H}, \hat{L}^z] = 0$

Table 3.1: Comparison between Fröhlich polaron and Angulon.

This implies one can use a similar method to solve the Angulon problem. In this chapter, we will introduce a variational study based on a single-excitation ansatz method. In the next chapter, we will propose a coherent state ansatz in the co-rotating frame to study the Angulon problem.

3.1.1 Derivation of Angulon Hamiltonian

Here we will derive the Angulon Hamiltonian from a general form:

$$\hat{H} = \hat{H}_{\rm r} + \hat{H}_{\rm b} + \hat{H}_{\rm i}. \tag{3.4}$$

The three terms respectively correspond to the rotational energy of the rotor, energy of the interacting bosonic bath, and rotor-boson interaction energy.

Rotor Hamiltonian

Usually, molecules are more complex than atoms. Molecules are composite particle systems. Apart from the usual electronic structures and external motion of nuclei, like translation and rotation of the center of mass, polyatomic molecules also contain additional internal structures, like the vibration and rotation. Fortunately, the electronic and vibrational transitions lie in energy regime ($10^{13} - 10^{14}$Hz and $10^{9} - 10^{11}$Hz) higher than the rotational transitions ($10^{9} - 10^{11}$Hz). Also, the low temperature and zero-viscosity of superfluid allow us to neglect the external motion of the molecule to high approximation. In rotational spectroscopy, we can assume molecules occupy the lowest electronic and vibrational state and only focus on the internal rotational degrees of freedom.

In this case, the rotating molecule can be modeled by a quantum rigid rotor [40, 42]:

$$\hat{H}_{\mathrm{r}} = \sum_{\alpha=x,y,z} B^{\alpha} (\hat{J}'^{\alpha})^2. \tag{3.5}$$

Here $\hat{J}'^{\alpha}$ is the angular momentum operator in the molecular (body-fixed) frame, which satisfies the anomalous commutation relations (More details are shown in the appendix). $\hat{J}'^{\alpha}$ transfers to the normal angular momentum (in lab-frame) $\hat{J}^{\alpha}$ by the rotational transformation, and the square is the same, $\hat{\boldsymbol{J}}^2 = \hat{\boldsymbol{J}}'^2$. B^{α} are the (bare) rotational constants, proportional to the inverse of moments of inertia, which characterize the molecular geometry. For example, $A = B = C$ corresponds to spherical tops (CCl_4); $A = B \neq C$ corresponds to symmetric tops (NH_3); $A = B; C = 0$ corresponds to linear molecules (CO_2). In this thesis, we will focus on the latter case, and the Hamiltonian is given by

$$\hat{H}_{\mathrm{r}} = B(\hat{J}'^{x})^2 + B(\hat{J}'^{y})^2 = B\hat{\boldsymbol{J}}^2. \tag{3.6}$$

Boson Hamiltonian

The superfluidity of ^{4}He originates from the gapless low-energy excitation, the phonon, in the interacting bosonic gas. The second-quantization

Hamiltonian is given by [43]

$$\hat{H}_{\mathrm{b}} = \sum_{\boldsymbol{k}} \epsilon_k \hat{a}^\dagger_{\boldsymbol{k}} \hat{a}_{\boldsymbol{k}} + \frac{1}{2} \sum_{\boldsymbol{k},\boldsymbol{k}',\boldsymbol{q}} V_{\mathrm{bb}}(\boldsymbol{q}) \hat{a}^\dagger_{\boldsymbol{k}'-\boldsymbol{q}} \hat{a}^\dagger_{\boldsymbol{k}+\boldsymbol{q}} \hat{a}_{\boldsymbol{k}'} \hat{a}_{\boldsymbol{k}}, \tag{3.7}$$

where $\sum_{\boldsymbol{k}} \equiv \int d^3\boldsymbol{k}/(2\pi)^3$. The first term represents the kinetic energy of bosons, where $\epsilon_k = k^2/2m$ and the bosonic operators in momentum space satisfy the commutation relation $[\hat{a}_{\boldsymbol{k}}, \hat{a}^\dagger_{\boldsymbol{k}'}] = (2\pi)^3 \delta(\boldsymbol{k} - \boldsymbol{k}')$. The second term represents the boson-boson interaction, and with the first-order Born approximation the interaction strength $V_{\mathrm{bb}}(\boldsymbol{q})$ reduces a constant $g_{\mathrm{bb}} = 4\pi a_{\mathrm{bb}}/m$.

The many-body Hamiltonian is hard to solve analytically. A standard way to simplify the Hamiltonian in the weakly-interacting and dilute limit is the Bogoliubov approximation and the Bogoliubov transformation [44]. After that the Hamiltonian reduces to a diagonal form:

$$\hat{H}_{\mathrm{b}} = \sum_{k\lambda\mu} \omega_k \hat{b}^\dagger_{k\lambda\mu} \hat{b}_{k\lambda\mu}, \tag{3.8}$$

where $\hat{b}^{(\dagger)}_{k\lambda\mu}$ are bosonic operators for the phonon excitation in the angular momentum basis, and the dispersion is given by

$$\omega_k = \sqrt{\epsilon_k(\epsilon_k + 2g_{\mathrm{bb}}n)}. \tag{3.9}$$

In the following, we will explain the derivation in detail. In a BEC, most of the atoms occupy the zero-momentum state. Therefore, one can interpret the bosonic operators as a macroscopic condensate at zero-momentum with addition to the finite-momentum fluctuations. Then, it is natural to split the sum over the full momentum space into two parts:

$$\hat{n} = \sum_{\boldsymbol{k}} \hat{a}^\dagger_{\boldsymbol{k}} \hat{a}_{\boldsymbol{k}} = \hat{a}^\dagger_{\boldsymbol{0}} \hat{a}_{\boldsymbol{0}} + \sum_{\boldsymbol{k}\neq 0} \hat{a}^\dagger_{\boldsymbol{k}} \hat{a}_{\boldsymbol{k}}. \tag{3.10}$$

Then the Hamiltonian turns into

$$\begin{aligned}
\hat{H}_{\mathrm{b}} =& \sum_{\boldsymbol{k}} \epsilon_k \hat{a}^\dagger_{\boldsymbol{k}} \hat{a}_{\boldsymbol{k}} + \frac{1}{2} g_{\mathrm{bb}} \sum_{\boldsymbol{k},\boldsymbol{k}',\boldsymbol{q}} \hat{a}^\dagger_{\boldsymbol{k}'-\boldsymbol{q}} \hat{a}^\dagger_{\boldsymbol{k}+\boldsymbol{q}} \hat{a}_{\boldsymbol{k}'} \hat{a}_{\boldsymbol{k}} \\
\approx& \frac{g_{\mathrm{bb}} n_{\boldsymbol{0}}^2}{2} + \sum_{\boldsymbol{k}\neq 0} (\epsilon_k + 2g_{\mathrm{bb}} n_0) \hat{a}^\dagger_{\boldsymbol{k}} \hat{a}_{\boldsymbol{k}} + \frac{g_{\mathrm{bb}} n_0}{2} \sum_{\boldsymbol{k}\neq 0} (\hat{a}^\dagger_{-\boldsymbol{k}} \hat{a}^\dagger_{\boldsymbol{k}} + \hat{a}_{-\boldsymbol{k}} \hat{a}_{\boldsymbol{k}}) \\
\approx& \frac{gn^2}{2} + \sum_{\boldsymbol{k}\neq 0} (\epsilon_k + g_{\mathrm{bb}} n) \hat{a}^\dagger_{\boldsymbol{k}} \hat{a}_{\boldsymbol{k}} + \frac{gn}{2} \sum_{\boldsymbol{k}\neq 0} (\hat{a}^\dagger_{-\boldsymbol{k}} \hat{a}^\dagger_{\boldsymbol{k}} + \hat{a}_{-\boldsymbol{k}} \hat{a}_{\boldsymbol{k}})
\end{aligned} \tag{3.11}$$

Here we only keep quadratic terms that are proportional to n, and neglect the higher interacting terms. And we assume the fluctuation to be small and the particle number in the zero-momentum condensate is close to the total particle number. Hence we can replace $\hat{a}_{\mathbf{0}}^{(\dagger)}$ by the square root of total particle number $\sqrt{n_0}$ and $n_0 \approx n$, and use the trick that $\hat{n}_0^2 \approx \hat{n}^2 - 2\hat{n}\sum_{\boldsymbol{k}\neq 0}\hat{a}_{\boldsymbol{k}}^\dagger \hat{a}_{\boldsymbol{k}}$. We further drop the constant term, then the Hamiltonian reduces to

$$\hat{H}_{\mathrm{b}} = \sum_{\boldsymbol{k}\neq 0}[\epsilon_k + g_{\mathrm{bb}}n]\hat{a}_{\boldsymbol{k}}^\dagger \hat{a}_{\boldsymbol{k}} + \frac{g_{\mathrm{bb}}n}{2}\sum_{\boldsymbol{k}\neq 0}[\hat{a}_{\boldsymbol{k}}^\dagger \hat{a}_{-\boldsymbol{k}}^\dagger + \hat{a}_{\boldsymbol{k}}\hat{a}_{-\boldsymbol{k}}]. \tag{3.12}$$

To diagonalize the Hamiltonian, we apply the Bogoliubov transformation:

$$\begin{aligned} \hat{a}_{\boldsymbol{k}} &= u_k \hat{b}_{\boldsymbol{k}} + v_{-k}^* \hat{b}_{-\boldsymbol{k}}^\dagger, \\ \hat{a}_{\boldsymbol{k}}^\dagger &= u_k^* \hat{b}_{\boldsymbol{k}}^\dagger + v_{-k} \hat{b}_{-\boldsymbol{k}}, \end{aligned} \tag{3.13}$$

where $\hat{b}_{\boldsymbol{k}}^{(\dagger)}$ are creation and annihilation operators for phonon excitations, and the coefficients satisfy the constraint, $|u_k|^2 - |v_{-k}|^2 = 1$.

Then the Hamiltonian becomes

$$\begin{aligned} \hat{H}_{\mathrm{b}} =& \sum_{\boldsymbol{k}\neq 0}[(\epsilon_k + g_{\mathrm{bb}}n)(|u_k|^2 + |v_k|^2) + g_{\mathrm{bb}}n(u_k^* v_k + u_k v_k^*)]\hat{b}_{\boldsymbol{k}}^\dagger \hat{b}_{\boldsymbol{k}} \\ &+ \sum_{\boldsymbol{k}\neq 0}[\frac{g_{\mathrm{bb}}n}{2}(u_k^* u_{-k}^* + v_{-k}^* v_k^*) + (\epsilon_k + g_{\mathrm{bb}}n)u_k^* v_{-k}^*]\hat{b}_{\boldsymbol{k}}^\dagger \hat{b}_{-\boldsymbol{k}}^\dagger + h.c. \\ \stackrel{!}{=}& \sum_{\boldsymbol{k}\neq 0}\omega_k \hat{b}_{\boldsymbol{k}}^\dagger \hat{b}_{\boldsymbol{k}} \end{aligned} \tag{3.14}$$

Here one can parameterize the coefficients by hyperbolic functions:

$$\begin{aligned} u_k &= \cosh\theta_k, \\ v_{-k} &= \sinh\theta_k. \end{aligned} \tag{3.15}$$

We require the off-diagonal term to vanish, which leads to

$$\frac{g_{\mathrm{bb}}n}{2}(v_{-k}v_k + u_k u_{-k}) + (\epsilon_k + g_{\mathrm{bb}}n)(u_k v_{-k}) \stackrel{!}{=} 0. \tag{3.16}$$

We thus obtain

$$\tanh 2\theta_k = -\frac{g_{\mathrm{bb}}n}{\epsilon_k + g_{\mathrm{bb}}n}, \tag{3.17}$$

and correspondingly,

$$\begin{aligned}\sinh 2\theta_k &= -\frac{g_{\rm bb}n}{\sqrt{(\epsilon_k+g_{\rm bb}n)^2-(g_{\rm bb}n)^2}},\\ \cosh 2\theta_k &= \frac{\epsilon_k+g_{\rm bb}n}{\sqrt{(\epsilon_k+g_{\rm bb}n)^2-(g_{\rm bb}n)^2}}.\end{aligned} \tag{3.18}$$

Then, the Bogoliubov dispersion relation is given by

$$\begin{aligned}\omega_k =& \cosh 2\theta_k[(\epsilon_k+g_{\rm bb}n)+g_{\rm bb}n\tanh 2\theta],\\ =&\sqrt{\epsilon_k(\epsilon_k+2g_{\rm bb}n)}.\end{aligned} \tag{3.19}$$

Furthermore, since we will deal with the angular momentum exchange between the rotor and the bath, it is more convenient to work in the angular momentum basis, whose transformation is given by

$$\hat{b}^\dagger_{\boldsymbol{k}} = \frac{(2\pi)^{3/2}}{k}\sum_{\lambda\mu}\hat{b}^\dagger_{k\lambda\mu}i^\lambda Y^*_{\lambda\mu}(\Theta_k,\Phi_k). \tag{3.20}$$

And the Hamiltonian turns to

$$\begin{aligned}\hat{H}_{\rm b} =& \sum_{\lambda\mu}\sum_{\lambda'\mu'}\int dk\omega_k(-1)^{\lambda'}i^{\lambda+\lambda'}\hat{b}^\dagger_{k\lambda\mu}\hat{b}_{k\lambda'\mu'}[\int d\Omega_{\boldsymbol{k}}Y^*_{\lambda\mu}(\Theta_k,\Phi_k)Y_{\lambda'\mu'}(\Theta_k,\Phi_k)]\\ \equiv&\sum_{k\lambda\mu}\omega_k\hat{b}^\dagger_{k\lambda\mu}\hat{b}_{k\lambda\mu}\end{aligned} \tag{3.21}$$

where $\sum_k \equiv \int dk$.

Rotor-Boson interaction

We consider a general form of rotor-boson interaction, given by:

$$\hat{H}_{\rm i} = \sum_{\boldsymbol{kq}} V_{\rm rb}(q,\hat{\phi},\hat{\theta},\hat{\gamma})\rho(\boldsymbol{q})\hat{a}^\dagger_{\boldsymbol{k}+\boldsymbol{q}}\hat{a}_{\boldsymbol{k}}, \tag{3.22}$$

where $\rho(\boldsymbol{q}) = e^{-i\boldsymbol{q}\cdot\boldsymbol{r}}$ is the Fourier transformation of the density of the impurity. Here we ignore the rotor's translational motion and assume that it is placed at $\boldsymbol{r}=0$. $(\hat{\phi},\hat{\theta},\hat{\gamma})$ are polar angle operators for the rotor.

We start deriving the interaction potential from a general form in the molecular frame, and expand in spherical harmonics:

$$V_{\rm rb}(\boldsymbol{r}) = \sum_{\lambda} V_{\lambda}(r) Y_{\lambda 0}(\theta_r, \phi_r). \tag{3.23}$$

Here we consider a linear rotor, thus only the $\mu = 0$ channel contributes. The z-axis is selected as the symmetry axis of the linear rotor, and the interaction strength only depends on the coordinates of bosons. Using the Wigner D-matrix, one can transfer the spherical harmonics to the lab frame:

$$Y_{\lambda 0}(\theta_r, \phi_r) = \sum_{\mu} D^{\lambda}_{\mu 0}(\hat{\theta}, \hat{\phi}, \hat{\gamma}) Y_{\lambda\mu}(\Theta_R, \Phi_R), \tag{3.24}$$

where $D^{\lambda}_{\mu 0}(\hat{\theta}, \hat{\phi}, \hat{\gamma}) = \sqrt{\frac{4\pi}{2\lambda+1}} Y^*_{\lambda\mu}(\hat{\theta}, \hat{\phi})$. Then, we reach the interaction potential in the lab frame:

$$V_{\rm rb}(\boldsymbol{R}, \hat{\theta}, \hat{\phi}) = \sum_{\lambda\mu} \sqrt{\frac{4\pi}{2\lambda+1}} Y^*_{\lambda\mu}(\hat{\theta}, \hat{\phi}) Y_{\lambda\mu}(\Theta_R, \Phi_R) V_{\lambda}(R), \tag{3.25}$$

where the distance between the rotor and bosons is independent of the frame, i.e. $R = r$. One can move to Fourier space:

$$\begin{aligned}
&V_{\rm rb}(\boldsymbol{k}, \hat{\theta}, \hat{\phi}) \\
=& \int d^3R V_{\rm rb}(\boldsymbol{R}, \hat{\theta}, \hat{\phi}) e^{i\boldsymbol{k}\cdot\boldsymbol{R}} \\
=& \sum_{\lambda\mu} \sum_{lm} \tilde{V}_{\lambda}(k) Y^*_{\lambda\mu}(\hat{\theta}, \hat{\phi}) Y_{lm}(\Theta_k, \Phi_k) [\int d\Omega_R Y_{\lambda\mu}(\Theta_R, \Phi_R) Y^*_{lm}(\Theta_R, \Phi_R)] \\
=& \sum_{\lambda\mu} \tilde{V}_{\lambda}(k) Y_{\lambda\mu}(\Theta_k, \Phi_k) \hat{Y}^*_{\lambda\mu}(\hat{\theta}, \hat{\phi}),
\end{aligned} \tag{3.26}$$

where $\tilde{V}_{\lambda}(k) \equiv \sqrt{\frac{4\pi}{2\lambda+1}}(4\pi) i^{-\lambda} \int dr r^2 V_{\lambda}(r) j_{\lambda}(kr)$ and we expand the exponential function as

$$e^{i\boldsymbol{k}\cdot\boldsymbol{R}} = \sum_{lm} (4\pi) i^{-l} j_l(kR) Y^*_{lm}(\Theta_R, \Phi_R) Y_{lm}(\Theta_k, \Phi_k). \tag{3.27}$$

Our next goal is to effectively describe the interaction Hamiltonian within the phonon picture. With the Bogoliubov approximation and transformation, we replace boson operators in the interaction Hamiltonian by the phonon operators:

$$\begin{aligned}\hat{H}_{\mathrm{i}} =& \sum_{\boldsymbol{kq}} V_{\mathrm{rb}}(\boldsymbol{q},\hat{\theta},\hat{\phi})\hat{a}^{\dagger}_{\boldsymbol{k}+\boldsymbol{q}}\hat{a}_{\boldsymbol{k}} \\ \approx& nV_{\mathrm{rb}}(0,\hat{\theta},\hat{\phi}) + \sqrt{n}\sum_{\boldsymbol{k}\neq 0} V_{\mathrm{rb}}(\boldsymbol{k},\hat{\theta},\hat{\phi})[\hat{a}^{\dagger}_{\boldsymbol{k}} + \hat{a}_{-\boldsymbol{k}}] \\ =& nV_{\mathrm{rb}}(0,\hat{\theta},\hat{\phi}) + \sqrt{n}\sum_{\boldsymbol{k}\neq 0} V_{\mathrm{rb}}(\boldsymbol{k},\hat{\theta},\hat{\phi})[(u^{*}_{k}+v^{*}_{k})\hat{b}^{\dagger}_{\boldsymbol{k}} + (u_{-k}+v_{-k})\hat{b}_{-\boldsymbol{k}}] \\ \rightarrow& \sqrt{n}\sum_{\boldsymbol{k}\neq 0} V_{\mathrm{rb}}(\boldsymbol{k},\hat{\theta},\hat{\phi})\sqrt{\frac{\epsilon_k}{\omega_k}}(\hat{b}^{\dagger}_{\boldsymbol{k}} + \hat{b}_{-\boldsymbol{k}}) \\ =& \sum_{k\lambda\mu} U_{\lambda}(k)[Y^{*}_{\lambda\mu}(\hat{\theta},\hat{\phi})\hat{b}^{\dagger}_{k\lambda\mu} + Y_{\lambda\mu}(\hat{\theta},\hat{\phi})\hat{b}_{k\lambda\mu}]\end{aligned} \tag{3.28}$$

Here we kke only terms to linear order. $\sum_k \equiv \int dk$ is the sum over the radial momentum $k = |\boldsymbol{k}|$, and the interaction strength is given by

$$U_{\lambda}(k) = [\frac{8nk^2\epsilon_k}{\omega_k(2\lambda+1)}]^{1/2}\int drr^2 V_{\lambda}(r)j_{\lambda}(kr), \tag{3.29}$$

where $V_{\lambda}(r) \equiv u_{\lambda}f(r)$ is usually obtained from approximate models or experimental data. Here we neglect the constant and quadratic terms.

3.2 Single-excitation ansatz

Several studies of the Angulon problems are based on a single-excitation ansatz [14, 17, 18, 45, 46], which is given by

$$|\psi_{LM}\rangle = Z^{1/2}|0\rangle|LM\rangle + \sum_{k\lambda\mu}\sum_{jn}\beta_{k\lambda j}C^{LM}_{jn,\lambda\mu}\hat{b}^{\dagger}_{k\lambda\mu}|0\rangle|jn\rangle. \tag{3.30}$$

Here $|0\rangle$ labels the bosonic vacuum, and Z is the quasiparticle renormalization factor satisfying the normalization condition, $|Z| + \sum_{k\lambda j}|\beta_{k\lambda j}|^2 = 1$. The first term indicates the non-interacting vacuum state. The second term

indicates the single-excitation state in which the Clebsch-Gordan coefficients $C^{LM}_{jn,\lambda\mu}$ incorporate the total angular momentum conservation of the rotor and excited phonons. The wavefunction is labeled by two quantum numbers, the total angular momentum quantum number L and its projection to the z axis M. It is easy to check that

$$\begin{aligned}\hat{\boldsymbol{L}}^2|\psi_{LM}\rangle &= L(L+1)|\psi_{LM}\rangle,\\ \hat{L}^z|\psi_{LM}\rangle &= M|\psi_{LM}\rangle.\end{aligned} \tag{3.31}$$

This ansatz, which reduces to the second-order perturbation theory at weak coupling, successfully explains the anomalous broadening of spectral lines in spectroscopy experiments [18], and the renormalization of rotational constants at weak coupling [17]. However, it fails to describe the renormalization of rotational constants in the intermediate-density regime.

In this section, we will reproduce some analytical results with the single-excitation ansatz. In the next chapter, we will propose a coherent state ansatz in the co-rotating frame and compare it with the single-excitation ansatz.

3.2.1 Variational methods

Based on the single-excitation ansatz, the variational energy is given by

$$E = \frac{\langle\psi_{LM}|\hat{H}|\psi_{LM}\rangle}{\langle\psi_{LM}|\psi_{LM}\rangle}, \tag{3.32}$$

which provides an estimate of the upper bound of ground state energy. Therefore, the goal is to minimize it and find the corresponding variational parameters, which is equivalent to minimize the functional, $F = \langle\psi_{LM}|(\hat{H}-E)|\psi_{LM}\rangle$.

First, one can calculate the expectation values term by term:

$$\begin{aligned}&\langle\psi_{LM}|\hat{H}_{\mathrm{r}}+\hat{H}_{\mathrm{b}}|\psi_{LM}\rangle\\ =&BL(L+1)|Z| + \sum_{k\lambda j}[\omega_k + Bj(j+1)]|\beta_{k\lambda j}|^2 \sum_{\mu m}(C^{LM}_{jm,\lambda\mu})^2\\ =&BL(L+1)|Z| + \sum_{k\lambda j} W_{kj}|\beta_{k\lambda j}|^2,\end{aligned} \tag{3.33}$$

and

$$\begin{aligned}
&\langle\psi_{LM}|\hat{H}_{\mathrm{i}}|\psi_{LM}\rangle \\
=&\sum_{k\lambda\mu}\sum_{jm}U_\lambda(k)C^{LM}_{jm,\lambda\mu}[Z^{1/2}\beta^*_{k\lambda j}\langle jm|Y^*_{\lambda\mu}(\hat{\theta},\hat{\phi})|LM\rangle + c.c.] \\
=&\sum_{k\lambda j}(-1)^\lambda V_\lambda(k)C^{j0}_{L0,\lambda 0}[Z^{1/2}(\beta_{k\lambda j})^* + c.c.]
\end{aligned} \tag{3.34}$$

where we introduce $V_\lambda(k) = \sqrt{\frac{2\lambda+1}{4\pi}}U_\lambda(k)$ and $W_{k\lambda} = \omega_k + B\lambda(\lambda+1)$ for compactness, and the spherical harmonics can be expanded in the angular momentum basis:

$$Y_{\lambda\mu}(\hat{\theta},\hat{\phi}) = \sum_{jm,j'm'} a^{j'm'}_{jm,\lambda\mu}|j'm'\rangle\langle jm|, \tag{3.35}$$

with

$$a^{j'm'}_{jm,\lambda\mu} = \sqrt{\frac{(2j+1)(2\lambda+1)}{(2j'+1)4\pi}}C^{j'm'}_{jm,\lambda\mu}C^{j'0}_{j0,\lambda 0}. \tag{3.36}$$

The Clebsch-Gordan coefficients satisfy the normalization condition $\sum_{\mu m}(C^{LM}_{jm,\lambda\mu})^2 = 1$ and the permutation rule

$$C^{jm}_{LM,\lambda-\mu} = (-1)^{\lambda-\mu}\sqrt{\frac{2j+1}{2L+1}}C^{LM}_{\lambda\mu,jm} = (-1)^{j-L-\mu}\sqrt{\frac{2j+1}{2L+1}}C^{LM}_{jm,\lambda\mu}. \tag{3.37}$$

We conclude the variational functional:

$$\begin{aligned}
F =&[BL(L+1) - E]|Z| + \sum_{k\lambda j}(W_{kj} - E)|\beta_{k\lambda j}|^2 \\
&+ \sum_{k\lambda j}(-1)^\lambda V_\lambda(k)C^{j0}_{L0,\lambda 0}[Z^{1/2}(\beta_{k\lambda j})^* + (Z^{1/2})^*\beta_{k\lambda j}].
\end{aligned} \tag{3.38}$$

One can find its minimum by determining the saddle point with respect to the variational parameters:

$$\frac{\delta F}{\delta(\beta_{k\lambda j})^*} = (W_{kj} - E)\beta_{k\lambda j} + (-1)^\lambda V_\lambda(k)C^{j0}_{L0,\lambda 0}Z^{1/2} \stackrel{!}{=} 0; \tag{3.39}$$

$$\frac{\delta F}{\delta(Z^{1/2})^*} = [BL(L+1) - E]Z^{1/2} + \sum_{k\lambda j}(-1)^\lambda V_\lambda(k)C^{j0}_{L0,\lambda 0}\beta_{k\lambda j} \stackrel{!}{=} 0. \tag{3.40}$$

The first equation provide a connection between the two variational parameters:

$$\frac{\beta_{k\lambda j}}{Z^{1/2}} = -\frac{(-1)^{\lambda} V_{\lambda}(k) C^{j0}_{L0,\lambda 0}}{W_{kj} - E}, \tag{3.41}$$

and the second results in a self-consistent equation for the variational energy:

$$\begin{aligned} E =& BL(L+1) + \sum_{k\lambda j} (-1)^{\lambda} V_{\lambda}(k) C^{j0}_{L0,\lambda 0} \frac{\beta^{LM}_{k\lambda j}}{Z^{1/2}_{LM}} \\ =& BL(L+1) - \Sigma_L(E), \end{aligned} \tag{3.42}$$

where one can introduce the 'self-energy':

$$\Sigma_L(E) = \sum_{k\lambda j} \frac{V^2_{\lambda}(k) (C^{j0}_{L0,\lambda 0})^2}{W_{kj} - E}. \tag{3.43}$$

As one can notice, after introducing the self-energy, one can rewrite the self-consistent equation in the Green's function language:

$$[G^0_L(E)]^{-1} - \Sigma_L(E) = 0, \tag{3.44}$$

where the free-particle Green's function of the rotor is defined as:

$$G^0_L(E) \equiv \frac{1}{BL(L+1) - E}, \tag{3.45}$$

whose pole corresponds to the free rotor energy.

The variational energy appears on the both sides of Eq. (3.44), then one can find its root numerically. After that, based on the normalization condiction and Eq. (3.41), one can derive the quasiparticle weight and the single-phonon wavefunction:

$$Z = [1 + \sum_{k\lambda j} \frac{V^2_{\lambda}(k) (C^{j0}_{L0,\lambda 0})^2}{(W_{kj} - E)^2}]^{-1}, \tag{3.46}$$

and

$$\beta_{k\lambda j} = -\frac{(-1)^{\lambda} V_{\lambda}(k) C^{j0}_{L0,\lambda 0}}{[(W_{kj} - E)^2 + \sum_{k\lambda j} V^2_{\lambda}(k) (C^{j0}_{L0,\lambda 0})^2]^{1/2}}, \tag{3.47}$$

which can be obtained by inserting the variational energy.

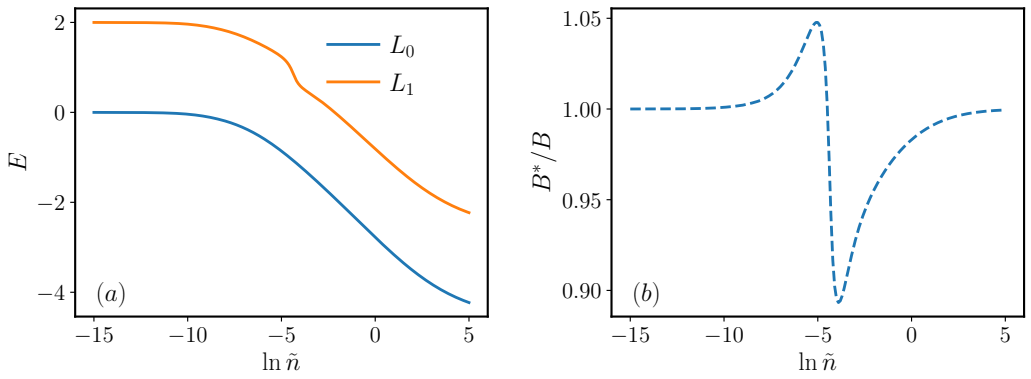

Figure 3.2: (a) Saddle point energy for $L = 0, 1$ sectors, which corresponds to the singular point of the Green's function, Eq. (3.48). (b) Effective rotational constants, as defined in Eq. (4.27).

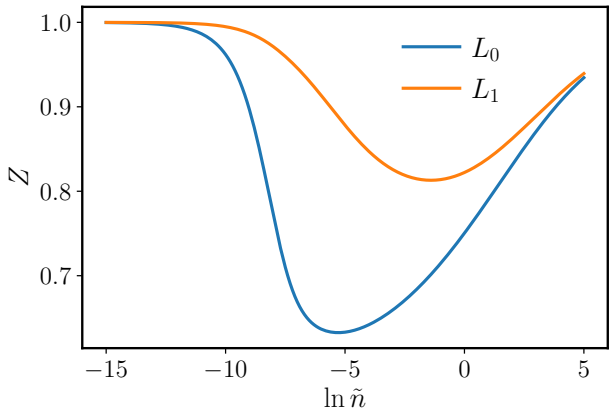

Figure 3.3: Quasiparticle weight for for $L = 0, 1$ sectors, which describe how well-defined the quasiparticle is.

In Fig. 3.2, we show the saddle point energy for $L = 0, 1$ sectors and the effective rotational constant. The single-excitation ansatz can describe well the rotational constants in the weak-coupling regime [17]. However, in the density-intermediate regime we shown, it yields an effective rotational constant exceeding one, implying that the bath causes the rotor to rotate faster, which is never observed in experiments. In Fig. 3.3, we show the quasiparticle weight for $L = 0, 1$ sectors, which decrease in the density-intermediate regime.

Next one can further introduce the Angulon Green's function:

$$G_L(E) = \frac{1}{BL(L+1) - E - \Sigma_L(E)}, \tag{3.48}$$

whose pole corresponds to the eigenenergy of the full Angulon Hamiltonian. It satisfies the Dyson equation:

$$G_L(E) = G_L^0(E) + G_L^0(E)\Sigma_L(E)G_L(E). \tag{3.49}$$

With the Green's function, one can access the excitation properties by calculating the spectral function, which is given by the imaginary part of the retarded Green's function:

$$A(\omega) = -\mathrm{Im}G_L^r(\omega) = -\mathrm{Im}G_L(\omega + i0^+). \tag{3.50}$$

The ground-state energy, excited-state energy, and quasiparticle properties can all be captured using the spectral function.

In Fig. 3.4, we show the spectral function obtained by the Green's function. Here the spectrum exhibits an instability regime, where the ground-state energy jumps, and a phonon wing, which is an excited-state branch splitting from the ground state. The instability regime, where ground-state energy jumps, accounts for the anomalous broadening of spectral lines. Experiments confirm the power of the single-excitation ansatz in describing the excited-state properties. However, the phonon wing has never been observed. We will propose an explanation in Chapter 5.

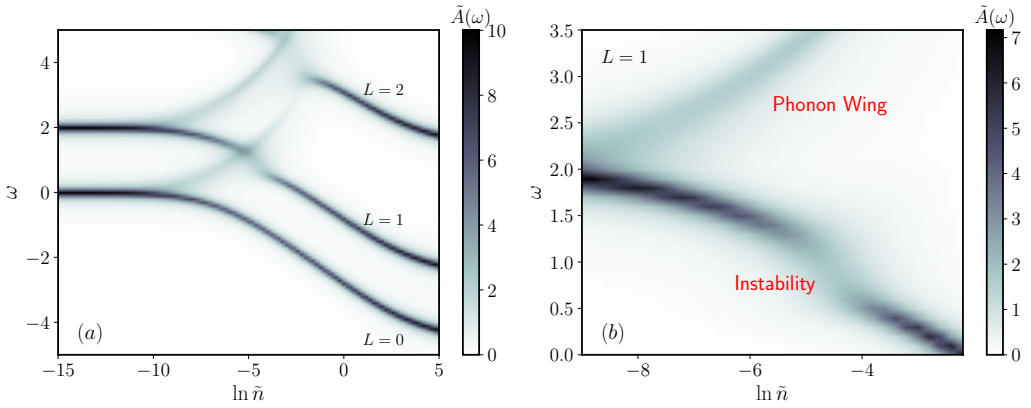

Figure 3.4: (a) Spectral function calculated from the Green's function for $L = 1, 2, 3$ sectors. (b) Zoom-in illustration of the spectral function for the $L = 1$ sector.

3.2.2 Real-time evolution of single-excitation ansatz

The spectral function, which is the imaginary part of the retarded Green's function, can be represented by the time evolution:

$$\begin{aligned} A(\omega) =& -\operatorname{Im} G_L^r(\omega) \\ =& 2\mathrm{Re} \int_0^{+\infty} dt G_L(t) e^{i\omega t}|_{\omega\to\omega+i0^+} \\ =& 2\mathrm{Re} \int_0^{+\infty} dt \langle\psi(0)|\psi(t)\rangle e^{i\omega t}|_{\omega\to\omega+i0^+} \end{aligned} \tag{3.51}$$

where the time-dependent Green's function is defined as overlap between the vacuum state and the time-dependent wavefunction and $|\psi(t)\rangle \equiv e^{-i\hat{H}t}|\psi(0)\rangle$. Then one can also access the spectral function by real-time evolution of the single-excitation ansatz. Next, we explain the derivation of the real-time evolution equations of motion, which will be useful in Chapter 5, when considering rotational spectroscopy.

We start from the Schrödinger equation for the single-excitation ansatz, $i\partial_t|\psi_{LM}\rangle = \hat{H}|\psi_{LM}\rangle$. The two sides are respectively written as:

$$i\partial_t|\psi_{LM}\rangle = i(\partial_t Z^{1/2}|0, LM\rangle + \sum_{k\lambda\mu}\sum_{jm}(\partial_t\beta_{k\lambda j})C^{LM}_{jm,\lambda\mu}|k\lambda\mu, jm\rangle); \tag{3.52}$$

$$\hat{H}|\psi_{LM}\rangle = Z^{1/2}\hat{H}|0,LM\rangle + \sum_{k\lambda\mu}\sum_{jm}\beta_{k\lambda j}C^{LM}_{jm,\lambda\mu}\hat{H}|k\lambda\mu,jm\rangle. \tag{3.53}$$

Utilizing the orthogonality of the basis and projecting them out, one can determine the equation of motion for variational parameters.

For the quasiparticle weight, one can project the Schrödinger equation onto $|0,LM\rangle$. The two sides read:

$$\text{l.h.s} = \langle 0,LM|i\partial_t|\psi_{LM}\rangle = i\partial_t Z^{1/2}_{LM}, \tag{3.54}$$

and

$$\begin{aligned}\text{r.h.s} =& Z^{1/2}\langle 0,LM|\hat{H}|0,LM\rangle + \sum_{k\lambda\mu}\sum_{jm}\beta_{k\lambda j}C^{LM}_{jm,\lambda\mu}\langle 0,LM|\hat{H}|k\lambda\mu,jm\rangle \\ =& BL(L+1)Z^{1/2}_{LM} + \sum_{k\lambda j}(-1)^{\lambda}V_{\lambda}(k)C^{j0}_{L0,\lambda 0}\beta^{LM}_{k\lambda j},\end{aligned} \tag{3.55}$$

where we use the fact that

$$\langle 0,LM|\hat{H}|0,LM\rangle = BL(L+1) \tag{3.56}$$

and

$$\langle 0,LM|\hat{H}|k\lambda\mu,jm\rangle = U_{\lambda}(k)\sqrt{\frac{(2j+1)(2\lambda+1)}{4\pi(2L+1)}}C^{L0}_{j0,\lambda 0}C^{LM}_{jm,\lambda\mu}. \tag{3.57}$$

For the single-excitation wavefunction, one can project the Schrödinger equation using $\sum_{\mu m} C^{LM}_{jm,\lambda\mu}\langle k\lambda\mu,jm|$. The two sides read:

$$\text{l.h.s} = \sum_{\mu m} C^{LM}_{jm,\lambda\mu}\langle k\lambda\mu,jm|i\partial_t|\psi_{LM}\rangle = i\partial_t\beta^{LM}_{k\lambda j}, \tag{3.58}$$

and

$$\begin{aligned}\text{r.h.s} =& \sum_{\mu m} C^{LM}_{jm,\lambda\mu}[Z^{1/2}\langle k\lambda\mu,jm|\hat{H}|0,LM\rangle \\ &+ \sum_{k'\lambda'\mu'}\sum_{j'm'}\beta_{k'\lambda'j'}C^{LM}_{j'm',\lambda'\mu'}\langle k\lambda\mu,jm|\hat{H}|k'\lambda'\mu',j'm'\rangle] \\ =& W_{kj}\beta^{LM}_{k\lambda j} + (-1)^{\lambda}V_{\lambda}(k)C^{j0}_{L0,\lambda 0}Z^{1/2}_{LM},\end{aligned} \tag{3.59}$$

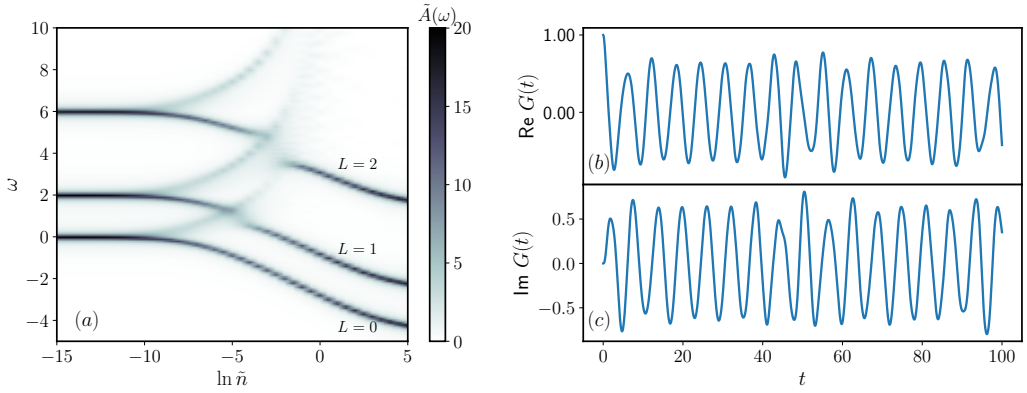

Figure 3.5: (a) Spectral function calculated by the real-time evolution. (b) The real and (c) the imaginary parts of the Green's function for $L = 0$ and $\ln\tilde{n} = -4.5$.

where we use the fact that

$$\langle k\lambda\mu, jm|\hat{H}|0, LM\rangle = U_\lambda(k)\sqrt{\frac{(2j+1)(2\lambda+1)}{4\pi(2L+1)}}C^{L0}_{j0,\lambda0}C^{LM}_{jm,\lambda\mu}, \tag{3.60}$$

and

$$\langle k\lambda\mu, jm|\hat{H}|k'\lambda'\mu', j'm'\rangle = [\omega_k + Bj(j+1)]\delta_{k\lambda\mu,k'\lambda'\mu'}\delta_{jm,j'm'}. \tag{3.61}$$

Therefore, we obtain the equations of motion for the variational parameters:

$$\begin{aligned} i\partial_t Z^{1/2} &= BL(L+1)Z^{1/2} + \sum_{k\lambda j}(-1)^\lambda V_\lambda(k)C^{j0}_{L0,\lambda0}\beta_{k\lambda j}, \\ i\partial_t\beta_{k\lambda j} &= W_{kj}\beta_{k\lambda j} + (-1)^\lambda V_\lambda(k)C^{j0}_{L0,\lambda0}Z^{1/2}. \end{aligned} \tag{3.62}$$

To study the spectral function, one needs the initial condition as input,

$$Z^{1/2}(t=0) = 1;\ \beta_{k\lambda j}(t=0) = 0, \tag{3.63}$$

and solve the ordinary differential equations.

As shown in Fig. 3.5, the numerical result agrees with the one calculated by Green's function. The advantage of real-time evolution is that numerical calculations are much easier and more efficient.

Chapter 4

Coherent State Ansatz

In the Fröhlich polaron, the Lee-Low-Pines (LLP) transformation can be used to decouple the impurity from the many-body bath. Then the remaining bosonic or fermionic model can be approximatively solved with a coherent state or Gaussian state ansatz. This method can be considered as a generalized mean-field theory. The overall variational wavefunction can be represented as a product state ansatz between the impurity and the bath with a canonical transformation, where the transformation entangles the two parts. This method thereby goes beyond the mean-field framework and results in the recently-developed non-Gaussian state methods [47]. As a result, even if one cannot always find the canonical transformation to decouple the impurity for more general impurity problems, one can still approximately use a canonical transformation to partially decouple it and then employ a variational ansatz.

In this chapter, we partially decouple the rotor using a rotational transformation. Then we introduce a product-state ansatz between a total angular momentum state for the whole system and a coherent state for the bosonic bath. One can optimize the variational parameters for one part by keeping the other fixed. We first examine the ground-state properties, such as the energy, effective rotational constants, and quasiparticle weights. Then we derive equations of motion for the real-time evolution, by which we compute the spectral function. This variational theory allows gaining insight into the system with a comprehensive wavefunction and a low computational cost.

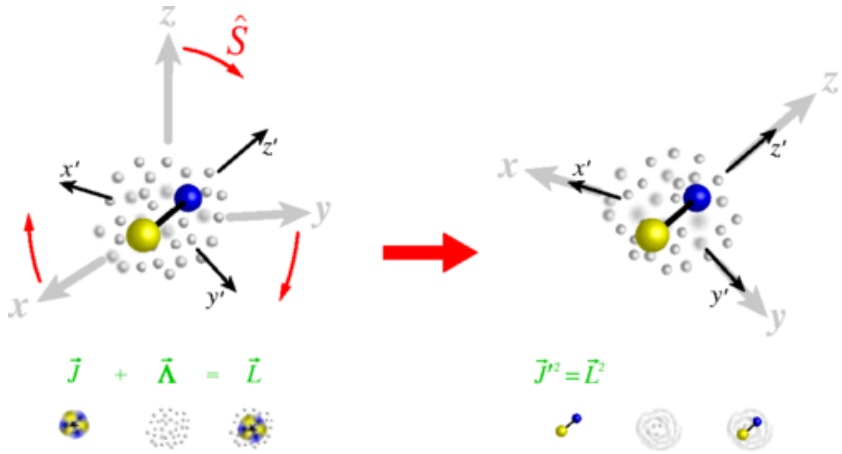

Figure 4.1: Schematic illustration for transforming to the molecular frame. Adapted from Ref. [15].

4.1 Variational ansatz

The LLP transformation is a translational transformation to the co-moving rame of the impurity that results from the total momentum conservation of the whole system. The Hamiltonian commutes with the total momentum operator, reducing the problems to purely bosonic or fermionic by considering given total momentum sectors, which is similar to block diagonalization of the Hamiltonian.

In the angulon system, similarly, the total angular momentum $\hat{L}_z$ and its squares $\hat{\boldsymbol{L}}^2$ are conserved. Analogous with the LLP transformation, the problem can be simplified by a rotation transformation (for an illustration see Fig. 4.1)) to the co-rotating frame, as shown in Ref. [15]:

$$\hat{S} = e^{-i\hat{\phi}\otimes\hat{\Lambda}^z} e^{-i\hat{\theta}\otimes\hat{\Lambda}^y} e^{-i\hat{\gamma}\otimes\hat{\Lambda}^z}. \tag{4.1}$$

Here we list some useful transformations:

$$\begin{aligned} \hat{S}^{-1}\hat{b}_{k\lambda\mu}\hat{S} &= \sum_{\nu} D^{\lambda}_{\mu\nu}(\hat{\phi},\hat{\theta},\hat{\gamma})\hat{b}_{k\lambda\mu}, \\ \hat{S}^{-1}(\sum_{\mu}\hat{b}^{\dagger}_{k\lambda\mu}\hat{b}_{k\lambda\mu})\hat{S} &= \sum_{\mu}\hat{b}^{\dagger}_{k\lambda\mu}\hat{b}_{k\lambda\mu}, \\ \hat{S}^{-1}\hat{\boldsymbol{J}}^2\hat{S} &= (\hat{\boldsymbol{J}}' - \hat{\boldsymbol{\Lambda}})^2, \end{aligned} \tag{4.2}$$

where $\hat{\boldsymbol{J}}'$ denotes the anomalous angular momentum operator, with the commutation relations:

$$[\hat{J}'^{\alpha}, \hat{J}'^{\beta}] = -i\epsilon_{\alpha\beta\gamma}\hat{J}'^{\gamma}. \tag{4.3}$$

Here the indices α, β, γ refer to the x, y, z components and $\epsilon_{\alpha\beta\gamma}$ is the Levi-Civita symbol. The anomalous angular momentum in the co-rotating frame represents the total angular momentum of the system.

The Hamiltonian in the rotating frame reads

$$\begin{aligned}\hat{\mathcal{H}} =&\hat{S}^{-1}\hat{H}\hat{S} = B(\hat{\boldsymbol{J}}' - \hat{\boldsymbol{\Lambda}})^2 \\ &+ \sum_{k\lambda\mu}\omega_k\hat{b}^{\dagger}_{k\lambda\mu}\hat{b}_{k\lambda\mu} + \sum_{k\lambda}V_{\lambda}(k)[\hat{b}^{\dagger}_{k\lambda 0} + \hat{b}_{k\lambda 0}],\end{aligned} \tag{4.4}$$

where $V_{\lambda}(k) = \sqrt{(2\lambda+1)/4\pi}U_{\lambda}(k)$.

The angular state is characterized by three quantum numbers, L, M and n, corresponding to the eigenvalues of operators, $\hat{\boldsymbol{J}}^2$, $\hat{J}^z$, and $\hat{J}'^z$, respectively, such that

$$\begin{aligned}\hat{\boldsymbol{J}}^2|LMn\rangle =&L(L+1)|LMn\rangle, \\ \hat{J}^z|LMn\rangle =&M|LMn\rangle, \\ \hat{J}'^z|LMn\rangle =&n|LMn\rangle,\end{aligned} \tag{4.5}$$

where $\hat{\boldsymbol{J}'}^2 = \hat{\boldsymbol{J}}^2$. Note that the system conserves the square of the angular momentum and the angular momentum projection to the lab frame, but not to the rotating frame.

In the slowly rotating limit, $B \to 0$, the Hamiltonian reduces to

$$\hat{\mathcal{H}}_{B=0} = \sum_{k\lambda\mu}\omega_k\hat{b}^{\dagger}_{k\lambda\mu}\hat{b}_{k\lambda\mu} + \sum_{k\lambda}V_{\lambda}(k)[\hat{b}^{\dagger}_{k\lambda 0} + \hat{b}_{k\lambda 0}], \tag{4.6}$$

which can be diagonalized exactly by a displacement operator,

$$\hat{U}^{\dagger}\hat{\mathcal{H}}_{B=0}\hat{U} = \sum_{k\lambda\mu}\omega_k\hat{b}^{\dagger}_{k\lambda\mu}\hat{b}_{k\lambda\mu} - \sum_{k\lambda}\frac{V^2_{\lambda}(k)}{\omega_k} \tag{4.7}$$

where $\hat{U} = \exp[-\sum_{k\lambda\mu}\frac{V_{\lambda}(k)}{\omega_k}(\hat{b}^{\dagger}_{k\lambda 0} - \hat{b}_{k\lambda 0})]$. The ground state is a coherent state which contains an infinite number of phonon excitations. The ground state energy reads $E_0 = -\sum_{k\lambda}V^2_{\lambda}(k)/\omega_k$.

Based on the above discussion, we propose a variational ansatz in the co-rotating frame:

$$|\psi\rangle = \sum_n g_n |LMn\rangle \otimes |C\rangle, \tag{4.8}$$

which is a product state between the angular state describing the total angular momentum, and bosonic coherent state describing the superfluid bath:

$$|C\rangle = \exp(\sum_{k\lambda\mu} \hat{b}^\dagger_{k\lambda\mu}\beta_{k\lambda\mu} - \hat{b}_{k\lambda\mu}\beta^*_{k\lambda\mu})|0\rangle, \tag{4.9}$$

where $|0\rangle$ stands for the vacuum state for bosons. Within a given L sector, one can substitute the operator $\hat{\boldsymbol{J}'}^2$ with its eigenvalue $L(L+1)$. Due to the non-commutation of $\hat{J'}^\alpha$, we consider a superposition in the n channel represented by the variational parameters g_n. As for the coherent bath, the $\beta_{k\lambda\mu}$ are the variational parameters, which are optimized by minimizing the variational energy. In dynamical problems, they are promoted to time-dependent variables. The ansatz is a mean-field theory in the transferred frame, while the overall ansatz in the lab frame, $\hat{S}|\psi\rangle$, includes the entanglement between the rotor and the bath through the canonical transformation $\hat{S}$. Hence our ansatz is beyond the mean-field framework.

While the coherent state ansatz has been discussed in Ref. [15, 17], it has not been considered as a variational state. In Ref. [17], is was shown to yield a phenomenological prediction to the renormalization of rotational constants in the strong-coupling regime, while in Ref. [15], one considers a single-excitation ansatz on top of a coherent bath, which exhibits a critical point where the impurity acquires one quantum of angular momentum from the many-particle bath. In these two papers, the displacement vector β is set as the exact solution for the $L = 0$ sector, where the rotor and phonon cloud do not rotate. In this thesis, the displacement is generalized to be variational parameters. As a result, we can take into account fully the phonon cloud's deformation caused by the rotor's rotation. Moreover, it is straightforward to extend the study the real-time evolution and dynamical problems.

Using Eq. (4.8), the variational energy reads:

$$\begin{aligned} E =& \langle\psi|\hat{\mathcal{H}}|\psi\rangle = BL(L+1) - 2B\boldsymbol{J'}\cdot\boldsymbol{\Lambda} + B\boldsymbol{\Lambda}\cdot\boldsymbol{\Lambda} \\ &+ \sum_{k\lambda\mu} W_{k\lambda}\beta^*_{k\lambda\mu}\beta_{k\lambda\mu} + \sum_{k\lambda} V_\lambda(k)(\beta^*_{k\lambda 0} + \beta_{k\lambda 0}) \end{aligned} \tag{4.10}$$

where $W_{k\lambda} \equiv \omega_k + B\lambda(\lambda+1)$, and the average quantities of angular momentum are given by

$$\begin{aligned} \Lambda^{\alpha} &\equiv \sum_{k\lambda\mu\nu} \beta^{*}_{k\lambda\mu}\sigma^{\lambda,\alpha}_{\mu\nu}\beta_{k\lambda\nu}, \\ J'^{\alpha} &\equiv \sum_{nn'} g^{*}_{n}g_{n'}\langle LMn|\hat{J}'^{\alpha}|LMn'\rangle. \end{aligned} \tag{4.11}$$

Here we use the properties of coherent state that

$$\hat{b}_{k\lambda\mu}|C\rangle = \beta_{k\lambda\mu}|C\rangle, \tag{4.12}$$

and

$$\begin{aligned} &\langle C|\hat{\mathbf{\Lambda}}^2|C\rangle \\ =&\sum_{\alpha}(\sum_{k\lambda\mu n}\sum_{m}\beta^{*}_{k\lambda\mu}\sigma^{\lambda,\alpha}_{\mu m}\sigma^{\lambda,\alpha}_{mn}\beta_{k\lambda n} + \sum_{k\lambda\mu\nu}\sum_{pjmn}\beta^{*}_{k\lambda\mu}\sigma^{\lambda,\alpha}_{\mu\nu}\beta_{k\lambda\nu}\beta^{*}_{pjm}\sigma^{j,\alpha}_{mn}\beta_{pjn}) \\ =&\sum_{k\lambda\mu}\lambda(\lambda+1)\beta^{*}_{k\lambda\mu}\beta_{k\lambda\mu} + \mathbf{\Lambda}\cdot\mathbf{\Lambda}. \end{aligned} \tag{4.13}$$

The next goal is minimizing the variational energy and obtaining the corresponding variational parameters.

4.2 Ground state

We employ a combined exact diagonalization and coherent state ansatz method to minimize the energy, similar to Ref. [48]. Within the product state structure, the angular and coherent states can be optimized iteratively. The scheme is to iteratively obtain ground states of the total angular momentum or the coherent bath with variational parameters of the other fixed. In the following, we will illustrate the optimization scheme in detail.

For the angular state, the effective Hamiltonian is obtained by tracing out the bosonic bath:

$$\hat{\mathcal{H}}_r = \langle C|\hat{\mathcal{H}}|C\rangle = -2B\mathbf{\Lambda}\cdot\hat{\boldsymbol{J}}' + f(\beta,\beta^{*}), \tag{4.14}$$

with

$$\begin{aligned} f(\beta,\beta^{*}) &= BL(L+1) + B\mathbf{\Lambda}\cdot\mathbf{\Lambda} \\ &+ \sum_{k\lambda\mu} W_{k\lambda}\beta^{*}_{k\lambda\mu}\beta_{k\lambda\mu} + \sum_{k\lambda} V_{\lambda}(k)(\beta^{*}_{k\lambda 0} + \beta_{k\lambda 0}). \end{aligned} \tag{4.15}$$

Remarkably, the effective model reduces to a single anomalous high-dimensional spin in an effective magnetic field $\boldsymbol{B}_{\text{eff}} = 2B\boldsymbol{\Lambda}$. The anomalous spin satisfies the anomalous commutation relations. The effective field, which is real, can be parameterized by its amplitude and two polar angles, $\boldsymbol{B}_{\text{eff}} = 2B(\Lambda^x, \Lambda^y, \Lambda^z) = |\boldsymbol{B}_{\text{eff}}|(\sin\theta\cos\phi, \sin\theta\sin\phi, \cos\theta)$. Here the effective field emerges from the rotation of the phonon bath and modifies the rotation of the rotor.

The Hamiltonian Eq. (4.14) can be represented in a matrix form and diagonalized numerically. We find that because the energy is minimized when the spin aligns with the effective field, one can diagonalize the Hamiltonian by a rotational transformation and obtain an expression for the ground state, which turns out to be the spin coherent state. Since we are, however, considering an anomalous spin, $\hat{\boldsymbol{J}}'$, the textbook results cannot be straightforwardly applied. However, similar techniques can still be employed. Here we introduce the rotational transformation for anomalous angular momentum:

$$\hat{D}'(\alpha, \beta, \gamma) = e^{-i\alpha\hat{J}'^z} e^{-i\beta\hat{J}'^y} e^{-i\gamma\hat{J}'^z}, \tag{4.16}$$

by which the Hamiltonian can be diagonalized, $\hat{D}'^\dagger(-\phi, -\theta, 0)\hat{\mathcal{H}}_r\hat{D}'^\dagger(-\phi, -\theta, 0) = -\hat{J}'^z$. The corresponding ground state is

$$\begin{aligned}
&\hat{D}'(-\phi, -\theta, 0)|LML\rangle \\
=&\sum_n |LMn\rangle\langle LMn|\hat{D}'(-\phi, -\theta, 0)|LML\rangle \\
=&\sum_n |LMn\rangle D'_{nL}(-\phi, -\theta, 0) \\
\equiv&\sum_n g_n|LMn\rangle,
\end{aligned} \tag{4.17}$$

where D'_{nm} is the Wigner D matrix. To avoid confusion with the normal spin coherent state, we refer to it the *anomalous spin coherent state*, whose superposition coefficients are given by

$$g_n = \binom{2L}{L+n}^{1/2} (\cos\frac{\theta}{2})^{L+n} (\sin\frac{\theta}{2})^{L-n} e^{-i\phi(L-n)}, \tag{4.18}$$

which is similar to the normal spin coherent state up to a phase. The detailed derivation is shown in Appendix B. The anomalous spin coherent states can

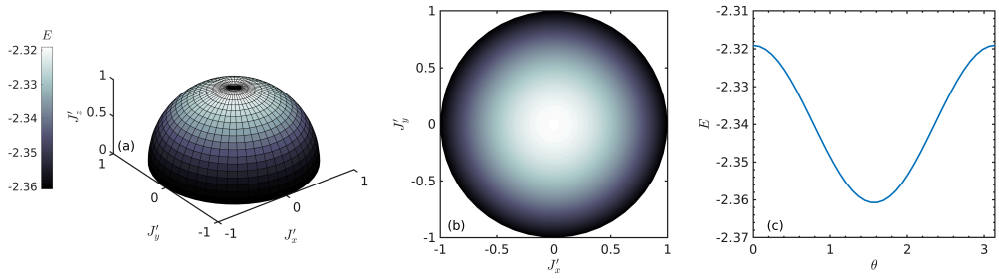

Figure 4.2: (a) Variational energy on the surface of Bloch sphere. The Bloch sphere is constructed by the vector field $\boldsymbol{J'}$ parameterized by the polar angles (θ, ϕ). (b) Projection of the variational energy into the $J'_x - J'_y$ plane. The energy is independent of ϕ and rotationally invariant about the J'_y axis. (c) Variational energy as a function of θ, which is minimized at the $\theta = \pi/2$.

be characterized by a vector, $\boldsymbol{J'}(\theta, \phi) = L(\sin\theta\cos\phi, \sin\theta\sin\phi, \cos\theta)$, pointing at the surface of the Bloch sphere as shown in Fig. 4.2(a). These states are macroscopic quantum states which minimize the variance of the angular momentum. Remarkably, it thus turns out that the ground state is described by a product state of the anomalous spin coherent state and the bosonic coherent states.

For the coherent bath, one can optimize the variational parameters by imaginary-time evolution:

$$\partial_\tau |C\rangle = -(\hat{\mathcal{H}}_b - E)|C\rangle \tag{4.19}$$

where $\hat{\mathcal{H}}_b = \sum_{nn'} g_n^* g_{n'} \langle LMn|\hat{\mathcal{H}}|LMn'\rangle$ is the effective Hamiltonian for bosons derived by tracing out the angular states. Correspondingly, one can derive the equation of motion for the variational parameters,

$$\partial_\tau \beta_{k\lambda\mu} = -\eta_{k\lambda\mu}, \tag{4.20}$$

with a mean-field Hamiltonian

$$\begin{aligned}\eta_{k\lambda\mu} =& W_{k\lambda}\beta_{k\lambda\mu} + \delta_{\mu 0} V_\lambda(k) \\ &+ 2B(\boldsymbol{\Lambda} - \boldsymbol{J'}) \cdot \sum_\nu \boldsymbol{\sigma}^\lambda_{\mu\nu} \beta_{k\lambda\nu}.\end{aligned} \tag{4.21}$$

For the sufficiently long evolution time, the variational energy converges to a local minimum, which is a saddle point of the mean-field Hamiltonian, i.e. $\eta_{k\lambda\mu} \stackrel{!}{=} 0$.

Above, we described the method to approach the local energy minimum for both angular and bosonic states by iteratively fixing the other. In this scheme, the angular momentum of bosons, $\mathbf{\Lambda}$, will evolve continuously in imaginary-time evolution, while the exact diagonalization of angular states can induce $\boldsymbol{J'}$ to have a sudden jump on the Bloch sphere. Finally, a global minimum will be reached when we perform the two processes iteratively.

An alternative approach is to find the saddle point in a self-consistent way. In Fig. 4.2, we first consider the angular states, and show the static energies obtained by fixing the angular momentum or the polar angles (θ, ϕ), and performing imaginary-time evolution for bosonic states. It indicates that energies are always minimized when $J'_z = 0$, correspondingly, $\theta = \pi/2$. This is because we consider a linear rotor, so that the rotation against the z axis should not have a favored direction. By symmetry, ϕ is irrelevant for the static problem. Hence without loss of generality, we set $\theta = \pi/2$ and $\phi = 0$ in the following ground-state calculation.

We next consider the bosonic states. In addition to solving the ordinary differential equations for imaginary-time evolution, the saddle point can be found in a self-consistent manner. For the ground state of the $L = 0$ sector, the total angular momentum vanishes, $\boldsymbol{J'} = 0$. Then a simple solution of the bosonic states follows:

$$\beta^{(0)}_{k\lambda\mu} = -\delta_{\mu 0} \frac{V_\lambda(k)}{W_{k\lambda}}, \tag{4.22}$$

with corresponding ground-state energy:

$$E_0 = -\sum_{k\lambda} \frac{V^2_\lambda(k)}{W_{k\lambda}}. \tag{4.23}$$

which is also referred to as deformation energy [15].

Also for general L sectors, the $\lambda = 0$ channel has a simple solution:

$$\beta_{k00} = -\frac{V_0(k)}{\omega_k}. \tag{4.24}$$

For the $\lambda = 1$ channel, one can write the mean-field Hamiltonian in a matrix

form:

$$\begin{pmatrix} W_{k1} & \sqrt{2}B(\Lambda^x - J'^x) & 0 \\ \sqrt{2}B(\Lambda^x - J'^x) & W_{k1} & \sqrt{2}B(\Lambda^x - J'^x) \\ 0 & \sqrt{2}B(\Lambda^x - J'^x) & W_{k1} \end{pmatrix} \otimes \begin{pmatrix} \beta_{k11} \\ \beta_{k10} \\ \beta_{k1-1} \end{pmatrix} = - \begin{pmatrix} 0 \\ V_1(k) \\ 0 \end{pmatrix}, \tag{4.25}$$

where we have taken $\Lambda^y = \Lambda^z = 0$ since $\theta = \pi/2$ and $\phi = 0$. From this one can derive the self-consistent equations:

$$\Lambda^x = \sum_k \frac{4BV_1^2(k)W_{k1}(J'^x - \Lambda^x)}{(W_{k1}^2 - 4B^2(J'^x - \Lambda^x)^2)^2}. \tag{4.26}$$

This equation can be solved numerically and one can then get the variational parameters $\beta_{k1\mu}$ by inserting Λ^x back to Eq. (4.25).

The renormalization of rotational constants is one of the most intriguing phenomena described by the angulon theory. It is similar to how a phonon cloud leads to the renormalization of the electron's mass in the Fröhlich model that describes the translational motion of a particle in a bosonic medium. In the angulon problem, the rotor excites a rotating phonon cloud and forms a quasiparticle. This deformation leads to a decreased effective rotational constant defined by

$$B^* = \frac{E_L - E_0}{L(L+1)}. \tag{4.27}$$

As a benchmark, we show the energy of the angulon for $L = 0, 1$ sectors in Fig. 4.3(a), and compared the effective rotational constants obtained by coherent state ansatz and single-excitation ansatz in Fig. 4.3(b). In the limit of both small and large densities, the results from the two approaches are consistent. However, in the intermediate regime, the single-excitation ansatz predicts an increasing effective rotational constant. This would indicate the surprising result of a 'speeding up' of the rotor which is both inconsistent with the physics of translational impuirities as well as experimental observations of molecules in superfluid Helium nanodroplets. On the contrary, the coherent state ansatz always predicts a decreasing rotational constant, indicating a consistent dressing of a polaron cloud that hinders the rotation of the composite state of the rotor and its local environment.

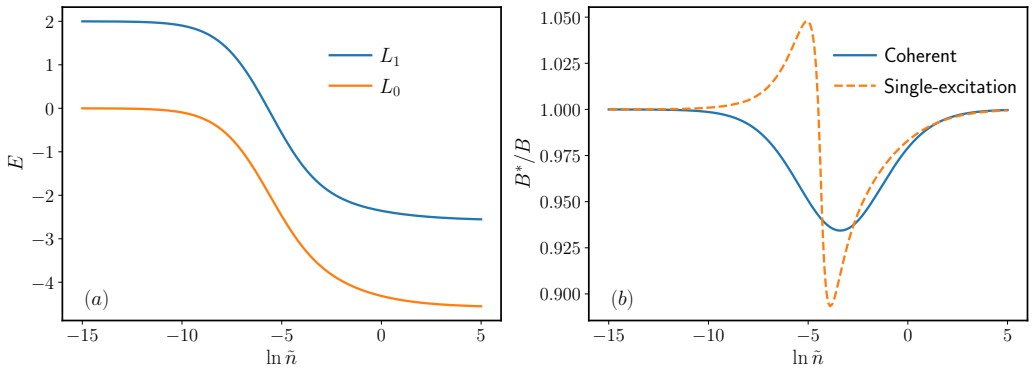

Figure 4.3: (a) Static energies E for $L = 0, 1$ sectors obtained by the coherent state ansatz, and (b) Effective rotational constants B^* obtained by the coherent state ansatz and single-excitation ansatz as a function of the dimensionless superfluid density $\tilde{n} = n(mB)^{-3/2}$. The results from the two ansatz are consistent at both small- and large-density regimes, but the single-excitation ansatz predicts an increasing effective rotational constant in the intermediate regime while the coherent state ansatz always predicts a decreasing one.

The quasiparticle weight Z is an important quasiparticle property, characterizing how well-defined the quasiparticle is. It is defined as the absolute square of the overlap between the vacuum state and the ground state, given by

$$Z = |\langle 0|C\rangle|^2 = e^{-N_{\mathrm{ph}}}, \tag{4.28}$$

where $N_{\mathrm{ph}} = \sum_{k\lambda\mu} |\beta_{k\lambda\mu}|^2$ indicates particle number of phonons. The weight Z determines how well-defined the quasiparticle is: when $Z > 0$, the quasiparticle is well-defined, whereas $Z = 0$ indicates the breakdown of the quasiparticle pictures akin to the 'orthogonality catastrophe' described in fermionic systems [49]. In Fig. 4.4, we show the quasiparticle weight and effective rotational constants as function of the rotor-boson interaction strength and superfluid density.

We note that for the coherent state ansatz, our theory breaks in the weakly-interacting regime for the $L \geq 2$ sectors. Technically speaking, this originates from the denominator of Eq. (4.26), which can reach a singular point, implying that the self-consistent equation does not guarantee a solu-

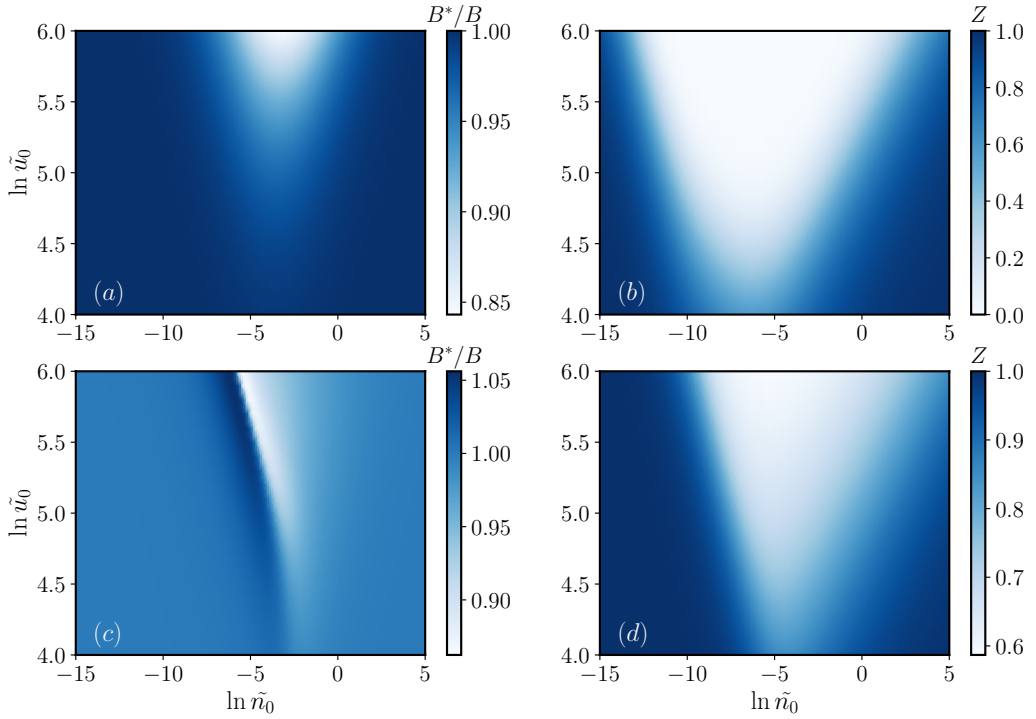

Figure 4.4: (a) and (c) are the effective rotational constants, and (b) and (d) are quasiparticle weights, obtained by the coherent state ansatz (top) and single-excitation ansatz (bottom) as a function of the superfluid density and the dimensionless rotor-boson interaction strength $\tilde{u}_0 = u_0/B$.

tion. This can be seen from the expression

$$\begin{aligned} &W_{k1}^2 - 4B^2(L-\Lambda^x)^2 \\ =&(\omega_k^2 + 2B\omega_k) - 4B^2[(L-\Lambda^x)^2 - 1]. \end{aligned} \tag{4.29}$$

When $(\omega_k^2 + 2B\omega_k) \geq 0$ and $[(L-\Lambda^x)^2 - 1] > 0$, Eq. (4.29) could be equal to zero as a function of k. Since $\Lambda^x \leq L$, it is always negative for $L = 0, 1$. For $L \geq 2$, however, it is only negative when Λ^x is large enough, which necessitates a strong interaction. Similar situation occurs when numerically conducting the imaginary-time evolution Eq. (4.20), in which the static variational parameter β turn out to be unphysical in the weakly-interacting regime for the $L \geq 2$. On the other hand, the Bogoliubov approximation is employed to derive the angulon model, then the model only involves the linear term

of rotor-phonon interaction. This approximation only works well when the interaction is weak. In addition, our approach considers an approximated product state structure between the angular state and the coherent state. For $L = 0$, the ansatz coincides with the exact ground state wavefunction since the dimension of angular state's Hilbert state is one. However, as L grows larger, the approximation becomes less accurate because more entanglement is required. In appendix C, we generalize our ansatz to a multimode coherent state, which further includes the entanglement between the angular momentum state and the bath.

4.3 Real-time evolution

We next consider the angulon spectral function obtained within the coherent state framework. The angulon Green's function is defined as $G(t) = \langle\psi(0)|\psi(t)\rangle$, where $|\psi(0)\rangle \equiv |LM0\rangle \otimes |0\rangle$ represents the unperturbed vacuum state, and $|\psi(t)\rangle = e^{-i\hat{\mathcal{H}}t}|\psi(0)\rangle$ indicates its time-evolution. The analytical structure of its Fourier transformation $G(\omega)$ in the complex frequency plane gives direct access to the angulon energy, lifetime, and quasi-particle weight. The quasiparticle spectral function is given by [50],

$$\begin{aligned} A(\omega) =& 2\mathrm{Re}\int_0^\infty dt e^{i\omega t}\langle\psi(0)|\psi(t)\rangle \\ =& 2\mathrm{Re}\int_0^\infty dt e^{i\omega t} g_0(t) e^{-\frac{1}{2}\sum_{k\lambda\mu}|\beta_{k\lambda\mu}(t)|^2}. \end{aligned} \tag{4.30}$$

Here we approximates the wavefunction $|\psi(t)\rangle$ with Eq. (4.8), and treat the variational parameters as time-dependent. The real-time evolution of $|\psi(t)\rangle$ is governed by the Schrödinger equation, $i\partial_t|\psi\rangle = \hat{H}|\psi\rangle$, from which one can derive the equations of motion for the variational parameters:

$$\begin{aligned} i\partial_t\beta_{k\lambda\mu} =& \delta_{\mu 0}V_\lambda(k) + W_{k\lambda}\beta_{k\lambda\mu} \\ &+ 2B(\boldsymbol{\Lambda} - \boldsymbol{J'})\cdot\sum_\nu \boldsymbol{\sigma}^\lambda_{\mu\nu}\beta_{k\lambda\nu}, \end{aligned} \tag{4.31}$$

and

$$\begin{aligned} i\partial_t g_n =& g_n[BL(L+1) + 2B\boldsymbol{J'}\cdot\boldsymbol{\Lambda} - B\boldsymbol{\Lambda}\cdot\boldsymbol{\Lambda} \\ &+ \sum_{k\lambda} V_\lambda(k)\mathrm{Re}\beta_{k\lambda 0}] - 2B\sum_{n'} g_{n'}\boldsymbol{J'}_{nn'}\cdot\boldsymbol{\Lambda}, \end{aligned} \tag{4.32}$$

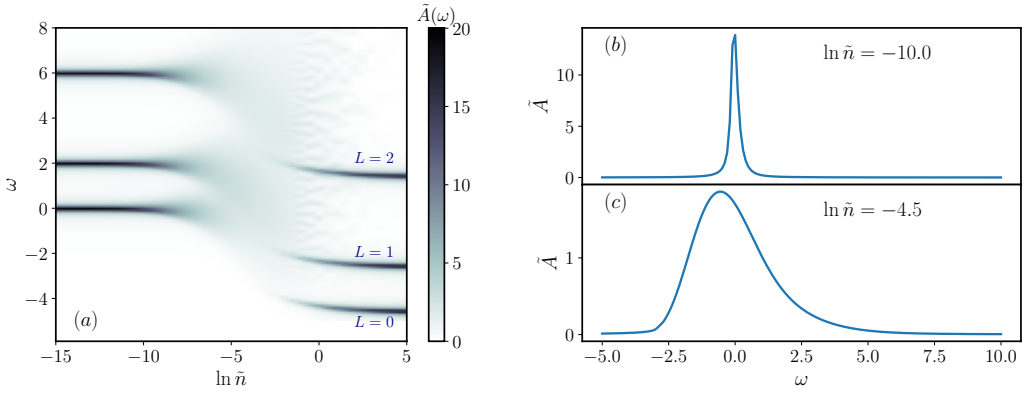

Figure 4.5: (a) Quasiparticle spectrum for $L = 1, 2, 3$ sectors against the superfluid density with coherent state ansatz. (b) and (c) are cuts of the spectrum function for $L = 0$ sector in small- and intermediate-density regimes.

where $\boldsymbol{J'}_{nn'} \equiv \langle LMn|\hat{\boldsymbol{J}}'|LMn'\rangle$.

Importantly, as the initial state $|\psi(0)\rangle$ is a zero-angular momentum state of the bosons, in the coherent state evolution the boson angular momentum $\boldsymbol{\Lambda}$ as well as $\boldsymbol{J'}$ remain zero in the evolution (unlike for the ground state which acquires finite expectation values of these quantities). As a result, the equation of motion reduce to a simple form:

$$\begin{aligned} i\partial_t \beta_{k\lambda\mu} &= \delta_{\mu 0} V_\lambda(k) + W_{k\lambda}\beta_{k\lambda\mu}, \\ i\partial_t g_n &= g_n[BL(L+1) + \sum_{k\lambda} V_\lambda(k)\mathrm{Re}\beta_{k\lambda 0}]. \end{aligned} \tag{4.33}$$

Due to this simplicity, the time evolution can be solved analytically and one obtains the analytical expressions for the variational parameters:

$$\beta_{k\lambda\mu}(t) = -\frac{\delta_{0\mu} V_\lambda(k)}{W_{k\lambda}}(1 - e^{-iW_{k\lambda}t}), \tag{4.34}$$

and

$$g_n(t) = \delta_{0,n} e^{-iBL(L+1)t} e^{i\sum_{k\lambda} V_\lambda^2(k)\frac{1-\mathrm{sinc}W_{k\lambda}t}{W_{k\lambda}}t}. \tag{4.35}$$

Fig. 4.5 (a) shows the spectral function as a function of the superfluid density. Compared to the single-excitation ansatz, the coherent state ansatz predicts a similar behavior at the small- and large-density regimes. However, the spectral function is dramaticallry broadened in the intermediate regime

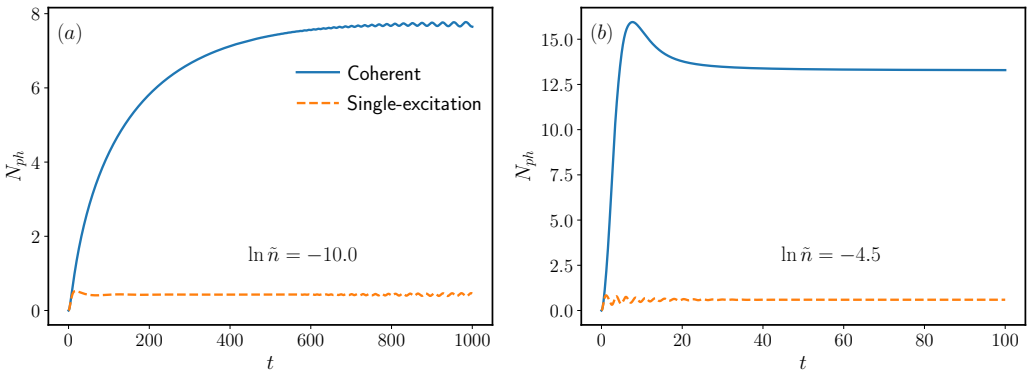

Figure 4.6: Real-time evolution of the average number of phonon excitations. The long-time oscillation originates from the discretion of radial momentum k.

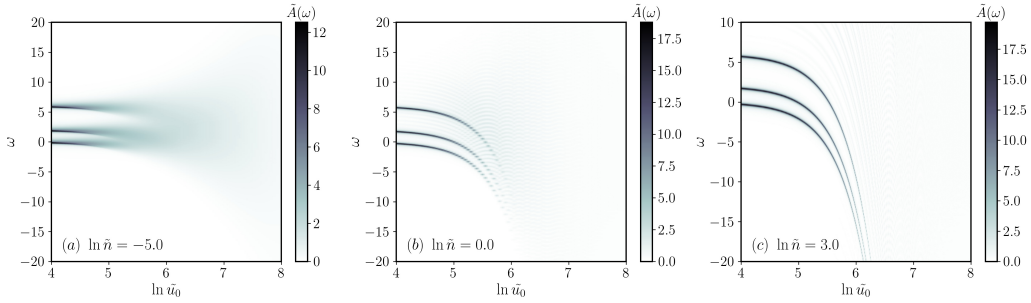

Figure 4.7: Quasiparticle spectrum against rotor-boson interaction strength corresponding to three density regimes.

even for the $L = 0$ sector, which is in agreement with the calculation of quasiparticle weights in 4.4 (b). In Fig. 4.5 (b) and (c), we show cuts of the spectral function in the small- and intermediate-density regimes, respectively. The angulon spectral line is sharp and high in the former case and is red-shifted and broadened for intermediate densities.

In Fig. 4.6 we compare the average number of phonon excitations obtained in evolution with the single-excitation ansatz for two density regimes. In the single-excitation ansatz the excitation number is limited to one by construction, while the coherent state does not impose such a limit and it indeed shows a growth of the phonon number to values significantly above 1.

In Fig. 4.7, we show the spectral function as function of the rotor-boson

interaction strength in three density regimes. In all cases, the spectral peaks are sharp at weak interaction and become unstable when increasing the interaction strength. Particularly, at large superfluid density and interaction strength, the spectral lines are significantly broadened.

Chapter 5

Rotational Spectroscopy

The transition energy between molecule's rotational states is experimentally studied using rotational spectroscopy, which involves applying a laser pulse to a molecule trapped in a superfluid nanodroplet. Often, the spectral function is used to interpret it theoretically:

$$\begin{aligned} A(\omega) =& 2\pi \sum_f |\langle f|0\rangle|^2 \delta(\omega - E_f) \\ =& \int_{-\infty}^{\infty} dt \langle 0|e^{-i\hat{H}t}|0\rangle e^{i\omega t}, \end{aligned} \tag{5.1}$$

where $|0\rangle$ represents the non-interacting vacuum state. Here the impurity itself is treated as the perturbation, and the spectral function describes the response of the sudden switching on of the impurity-bath interaction. The spectral function provides a direct estimate of how well-defined the quasiparticle is, thereby we will refer to it as quasiparticle spectrum to avoid misunderstanding.

The spectral function can be numerically calculated using the single-excitation ansatz, as described in Chapter 3. The angulon instability region in the spectral function explains the anomalous broadening of the spectral lines in experiments. However, the phonon wings, which dominate in the instability regime, have never been observed in rotational spectroscopy. This casts question on the validity of the single-excitation approach.

In this chapter, we will use Fermi's golden rule to examine the rotational spectroscopy more carefully. We consider both the coherent state ansatz and the single-excitation ansatz, taking into account the laser perturbation and the equilibrium initial states.

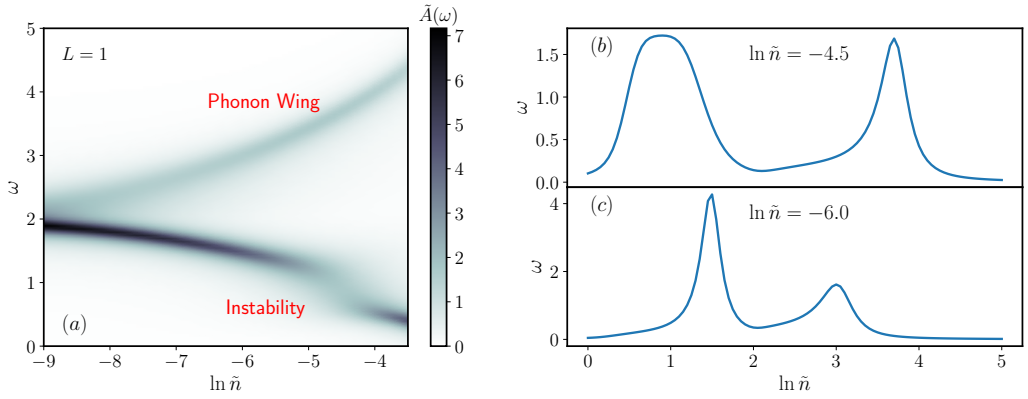

Figure 5.1: (a) Spectral function for $L = 1$ obtained by the single-excitation ansatz. (b) Cuts of the spectral lines.

5.1 Absorption spectrum

In actual chemistry experiments, instead of a rapid injection, the molecule is prepared in equilibrium with the nanodroplet. The molecule will then be excited to higher angular momentum channels by a laser pulse. Therefore, the considerable way is to apply Fermi's golden rule, which is given by

$$\begin{aligned} A_a(\omega) =& 2\pi \sum_f |\langle f|\hat{V}|i\rangle|^2 \delta(\omega - E_f + E_i) \\ =& \sum_f \langle i|\hat{V}|f\rangle\langle f|\hat{V}|i\rangle \int_{-\infty}^{\infty} dt e^{i(\omega - E_f + E_i)t} \\ =& \int_{-\infty}^{\infty} dt \langle i|\hat{V} e^{-i\hat{H}t}\hat{V}|i\rangle e^{i(\omega+E_i)t}. \end{aligned} \tag{5.2}$$

Here the "initial" state, $|i\rangle$, represents the ground state of Angulon instead of the vacuum state in the quasiparticle spectrum in Eq. (4.30), and E_i denotes the ground state energy. $\hat{V}$ is the amplitude of harmonic perturbation $\hat{\mathcal{V}}(t) = \hat{V}(e^{i\omega t} + e^{-i\omega t})$. We assume a dipole-field interaction between the molecule and the electric field. The first-order effect dominates for dipolar molecules, and the interaction is given by $-\hat{\boldsymbol{d}} \cdot \boldsymbol{\mathcal{E}}(t) \approx -\mu_0 \mathcal{E}_0 \cos\omega t \cos\hat{\theta}$. Here μ_0 is the dipole moment of the molecule and $\mathcal{E}_0$ is the amplitude of the electric field. Then the laser perturbation reads $\hat{V} = -\mu_0 \mathcal{E}_0 \cos\hat{\theta}$, resulting in $L = 0 \to 1$ transitions.

This perturbation only excites the rotor state and does not modify the variational manifolds for both the two ansatzes, which will be illustrated in detail in the following two sections. In brief, we label the ground state in the $L = 0$ channel as $|\psi_{00}\rangle$, where the second index indicates M for the single-excitation ansatz and n for the coherent state ansatz. The perturbation can be written as

$$\hat{V} \sim \cos\hat{\theta} = \sqrt{\frac{4\pi}{3}} Y_{10}(\hat{\theta}), \tag{5.3}$$

which can be expanded in the angular momentum basis. It excites the ground state to the $L = 1$ sector, such that $\cos\hat{\theta}|\psi_{00}\rangle \equiv \sqrt{\frac{1}{3}}|\psi'_{10}\rangle$, where $|\psi'_{10}\rangle$ labels an unnormalized state for both the single-excitation ansatz and coherent state ansatz with the quantum number $L = 1$. For convenience, we can get rid of the amplitude of perturbation by introducing

$$\begin{aligned} \tilde{A}_a(\omega) \equiv & \frac{3}{(\mu_0 \mathcal{E}_0)^2} A_a(\omega) \\ = & \int_{-\infty}^{\infty} dt \langle \psi'_{10}(0)|\psi'_{10}(t)\rangle e^{i(\omega+E_0)t}, \end{aligned} \tag{5.4}$$

where E_0 indicates the ground state energy. Therefore, since the equations of motions still hold, one can numerically calculate the absorption spectrum by real-time evolution. We will next illustrate the calculation for both the coherent state ansatz and single-excitation ansatz.

5.2 Coherent states

We first focus on the coherent states ansatz. The ground-state ansatz in the laboratory frame is given by

$$\hat{S}(|000\rangle \otimes |C_0\rangle) \equiv \hat{S}|\psi_{00}\rangle. \tag{5.5}$$

It is worth mentioning that the $\cos\hat{\theta}$ perturbation is invariant under the rotational transformation, $[\hat{S}, \hat{V}] = 0$. Then the spectrum can be written as

$$\begin{aligned} A_a(\omega) &= \int_{-\infty}^{\infty} dt \langle \psi_{00}|\hat{S}^\dagger \hat{V} e^{-i\hat{H}t} \hat{V} \hat{S}|\psi_{00}\rangle e^{i(\omega+E_0)t} \\ &= \int_{-\infty}^{\infty} dt \langle \psi_{00}|\hat{V} \hat{S}^\dagger e^{-i\hat{H}t} \hat{S} \hat{V}|\psi_{00}\rangle e^{i(\omega+E_0)t} \\ &= \int_{-\infty}^{\infty} dt \langle \psi_{00}|\hat{V} e^{-i\hat{\mathcal{H}}t} \hat{V}|\psi_{00}\rangle e^{i(\omega+E_0)t}. \end{aligned} \tag{5.6}$$

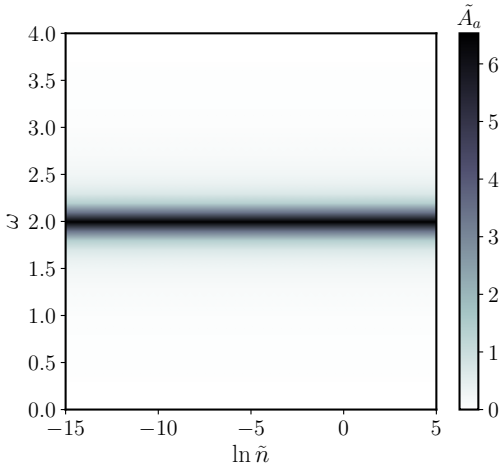

Figure 5.2: Rotational spectroscopy obtained by the coherent state ansatz.

In the last line, the Hamiltonian is replaced by the one in the transferred frame, Eq. (4.4). Next one can apply the perturbation to the ground state:

$$\begin{aligned}
&\hat{V}|\psi_{00}\rangle \\
\sim &\cos\hat{\theta}(|000\rangle|C_0\rangle) \\
= &\sum_{jmn}\sqrt{\frac{1}{2j+1}}C^{jn}_{00,10}C^{jm}_{00,10}|jmn\rangle|C_0\rangle \\
= &\sqrt{\frac{1}{3}}|100\rangle|C_0\rangle,
\end{aligned} \tag{5.7}$$

where $C^{j'm'}_{00,20} = \delta_{j'2}\delta_{m'0}$. One can label $|\psi'_{10}(t=0)\rangle = |100\rangle|C_0\rangle$, which has the same form as the variational ansatz with $L = 1$.

The ground-state wavefunction and energy have been shown in Eq. (4.22) and Eq. (4.23). We then calculate the rotational spectroscopy in Fig. 5.2. Surprisingly, even though the coherent state predicts a rich spectral function in the intermediate-density regime as shown in Fig. 4.5, the corresponding rotational spectroscopy is trivial.

Technically speaking, this is caused by the fact that the mean values of the angular momentum operators $\hat{\mathbf{\Lambda}}$ and $\hat{\boldsymbol{J}}'$ for the initial state $|100\rangle|C_0\rangle$ are equal to zero in the evolution, rendering the time evolution trivial. For the

coherent state, the time evolution reduce to

$$i\partial_t \beta_{k\lambda\mu}(t=0) = \delta_{\mu 0} V_\lambda(k) + W_{k\lambda}\beta_{k\lambda\mu}(t=0) = 0, \tag{5.8}$$

where $\beta_{k\lambda\mu}(t=0) = -\delta_{\mu 0}\frac{V_\lambda(k)}{W_{k\lambda}}$. Therefore, it does not evolve. As for the angular state, with the constraint of $\mathbf{\Lambda} = 0$, the equation of motion reduces to a linear ordinary differential equation:

$$i\partial_t g_n = g_n[BL(L+1) + \sum_{k\lambda} V_\lambda(k)\mathrm{Re}\beta_{k\lambda 0}]. \tag{5.9}$$

Hence, only the $n = 0$ channel survives and evolves up to a phase. Thus the energy in the time-evolution does not change:

$$\begin{aligned} E =& \frac{\langle\psi'_{10}|\hat{\mathcal{H}}|\psi'_{10}\rangle}{\langle\psi'_{10}|\psi'_{10}\rangle} \\ =& E_0 + BL(L+1) \end{aligned} \tag{5.10}$$

and the spectral function,

$$\tilde{A}_a(\omega) = \int_{-\infty}^{\infty} dt e^{i(\omega - BL(L+1))t}, \tag{5.11}$$

has a trivial structure with the coherent state approach, which is thus clearly insufficient to capture the physics of rotational spectroscopy experiments.

5.3 Single-excitation ansatz

We next examine the single-excitation ansatz. The self-consistent calculations in Chapter 3 yields the following ground-state variational parameters:

$$\begin{aligned} Z_{(0)}^{1/2} =& [1 + \sum_{k\lambda} \frac{V_\lambda^2(k)}{(W_{k\lambda} - E_0)^2}]^{-1}, \\ \beta_{k\lambda\lambda}^{(0)} =& (-1)^{\lambda+1}\frac{V_\lambda(k)}{W_{k\lambda} - E_0} Z_{(0)}^{1/2}, \end{aligned} \tag{5.12}$$

which can be numerically obtained by inserting the ground state energy E_0. Then, one can calculate the laser perturbation acting on this state:

$$\begin{aligned}
&\hat{V}|\psi_{00}\rangle \\
&\sim \cos\hat{\theta}(Z_{(0)}^{1/2}|0\rangle|00\rangle + \sum_{k\lambda\mu}\beta_{k\lambda\lambda}^{(0)}\frac{(-1)^{\lambda+\mu}}{\sqrt{2\lambda+1}}|k\lambda\mu\rangle|\lambda,-\mu\rangle) \\
&=\sum_{jm}(Z_{(0)}^{1/2}\sqrt{\frac{1}{2j+1}}C_{00,10}^{jm}C_{00,10}^{jm}|0\rangle|jm\rangle + \sum_{k\lambda\mu}\beta_{k\lambda\lambda}^{(0)}\frac{(-1)^{\lambda+\mu}}{\sqrt{2j+1}}C_{\lambda0,10}^{j0}C_{\lambda-\mu,10}^{jm}|k\lambda\mu\rangle|jm\rangle) \\
&=\sum_{jm}(Z_{(0)}^{1/2}\sqrt{\frac{1}{2j+1}}\delta_{jm,10}|0\rangle|jm\rangle + \sum_{k\lambda\mu}\beta_{k\lambda\lambda}^{(0)}\frac{(-1)^{\lambda+\mu}}{\sqrt{2j+1}}C_{\lambda0,10}^{j0}C_{\lambda-\mu,10}^{jm}|k\lambda\mu\rangle|jm\rangle) \\
&=\sqrt{\frac{1}{3}}(Z_{(0)}^{1/2}|0\rangle|10\rangle + \sum_{k\lambda\mu}\sum_{jm}(-1)^{\lambda}\sqrt{\frac{2j+1}{3}}\beta_{k\lambda\lambda}^{(0)}C_{j0,\lambda0}^{10}C_{jm,\lambda\mu}^{10}|k\lambda\mu\rangle|jm\rangle) \\
&=\sqrt{\frac{1}{3}}(Z_{(0)}^{1/2}|0\rangle|10\rangle + \sum_{k\lambda\mu}\sum_{jm}\beta'_{k\lambda j}C_{jm,\lambda\mu}^{10}|k\lambda\mu\rangle|jm\rangle) \\
&=\sqrt{\frac{1}{3}}|\psi'_{10}\rangle.
\end{aligned} \tag{5.13}$$

Here we introduced

$$|\psi'_{10}\rangle \equiv Z_{(0)}^{1/2}|0\rangle|10\rangle + \sum_{k\lambda\mu}\sum_{jm}\beta'_{k\lambda j}C_{jm,\lambda\mu}^{10}|k\lambda\mu\rangle|jm\rangle, \tag{5.14}$$

where the single-excitation wavefunction is defined as

$$\beta'_{k\lambda j} = (-1)^{\lambda}\sqrt{\frac{2j+1}{3}}\beta_{k\lambda\lambda}^{(0)}C_{j0,\lambda0}^{10}. \tag{5.15}$$

The wavefunction $|\psi'_{10}\rangle$ respects the form of the single-excitation ansatz, hence the equations of motions also obey:

$$\begin{aligned}
i\partial_t Z^{1/2} &= BL(L+1)Z^{1/2} + \sum_{k\lambda j}(-1)^{\lambda}V_{\lambda}(k)C_{L0,\lambda0}^{j0}\beta_{k\lambda j}, \\
i\partial_t\beta_{k\lambda j} &= W_{kj}\beta_{k\lambda j} + (-1)^{\lambda}V_{\lambda}(k)C_{L0,\lambda0}^{j0}Z^{1/2},
\end{aligned} \tag{5.16}$$

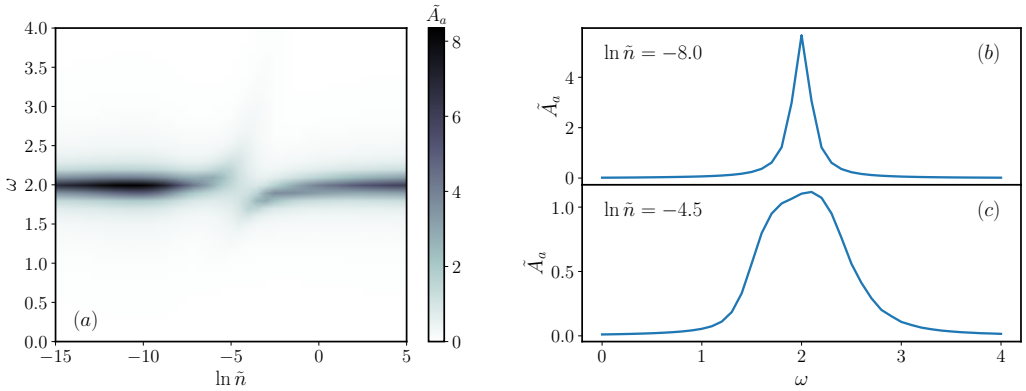

Figure 5.3: Rotational spectroscopy obtained by (a) the single-excitation ansatz. (b) and (c) are cuts of spectral lines from the single-excitation ansatz in the small- and intermediate-density regimes.

with initial conditions given by

$$\begin{aligned} Z^{1/2}(0) =& Z^{1/2}_{(0)}, \\ \beta_{k\lambda j}(0) =& \beta'_{k\lambda j} \equiv (-1)^{\lambda}\sqrt{\frac{2j+1}{3}}\beta^{(0)}_{k\lambda\lambda}C^{10}_{j0,\lambda 0}. \end{aligned} \tag{5.17}$$

In Fig. 5.3 (a), the rotational spectroscopy still reproduces an instability regime, while remarkably the phonon wing is not observed. Fig. 5.3 (c) shows the spectral line at the intermediate-density regime. In the instability regime, the quasiparticle is unstable and the spectral lines are significantly broadened, as observed in experiments [7, 18]. The spectral line in the small-density regime is sharp as shown in Fig. 5.3 (b), in contrast to the quasiparticle spectral function shown in Fig 5.1, where the spectral line splits into two.

The phonon wing is understood as an excited-state branch. Here the laser, which only interacts with the rotor, excites the ground state to the lower branch of the $L = 1$ sector. The redistribution of the angular momentum between rotor and bath is not strong enough to jump to the upper branch. In other word, the wavefunction for the upper branch has no overlap with the state $|\psi'_{10}\rangle$.

Initial States

As mentioned above, if the laser perturbation and the equilibrium initial-state are correctly taken into account, the spectral function exhibits an instability regime but no phonon wings, which is consistent with rotational spectroscopy experiments. The importance of the perturbation is obvious since different types of perturbations correspond to different experimental setups. For example, in electronic spectroscopy experiments, both the molecule and bath are excited, and both the instability regime and phonon wings are observed [3].

The equilibrium initial-state also plays a key role in compressing the phonon wings. This can be demonstrated by performing the calculation for a vacuum initial state:

$$\begin{aligned} &\hat{V}|0\rangle|00\rangle \\ \sim &\cos\hat{\theta}(|0\rangle|00\rangle) \\ = &\sum_{jm}\sqrt{\frac{1}{2j+1}}C^{j0}_{00,10}C^{jm}_{00,10}|0\rangle|jm\rangle \\ = &\sqrt{\frac{1}{3}}|0\rangle|10\rangle. \end{aligned} \tag{5.18}$$

Here $|\psi^{(0)}_{10}\rangle = |0\rangle|10\rangle$ is the vacuum state at $L = 1$ up to a constant coefficient. In this case, the absorption spectrum is given by

$$\tilde{A}_a(\omega) \equiv = \int_{-\infty}^{\infty} dt\langle\psi^{(0)}_{10}|e^{-i\hat{H}t}|\psi^{(0)}_{10}\rangle e^{i(\omega+E_0)t}, \tag{5.19}$$

which is the same as the quasiparticle spectrum for $L = 1$ sector up to a shift. Hence the phonon wings will still appear.

This discussion points out the importance of equilibrium initial state, and also suggests a way to observe a phonon wing in rotational spectroscopy. For rotational spectroscopy, the type of perturbation is fixed, but one can consider a non-equilibrium initial state. For example, one can turn on the laser pulse before the molecule reaches equilibrium with the bath.

Chapter 6

Conclusion and Outlook

Conclusion

In this thesis, we variationally studied the angulon model, which is an effective description for an isolated molecule immersed in a superfluid matrix. We intended to resolve the two issues raised in previous research: (1) a proper interpretation for the effective rotational constants and (2) finding an explanation for the unobservable phonon wings in rotational spectroscopy experiments.

We began the discussion by introducing the Fröhlich polaron model in Chapter 2. The Fröhlich polaron, formed by a moving electron dressed by phonons, is a paradigm for quasiparticles and also quantum impurity problems. Historically, many methods have been proposed for its solution. In this thesis, we revisited perturbation theory and the Lee-Low-Pines method. Perturbation theory provides a good approximation in the weak-coupling regime for a wide range of fields. The second-order perturbation wavefunction, a superposition of a vacuum state and a single-phonon excitation state, can be generalized into a variational ansatz. As for the Lee-Low-Pines method, it first decouples the impurity with a canonical transformation and then solves the pure bosonic model with a coherent state ansatz. These two methods construct toolboxes for solving the angulon model.

The angulon model was introduced in Chapter 3. The molecule is approximated as a quantum rigid rotor, as only its rotational degrees of freedom are involved in rotational spectroscopy. One can subsequently construct a generic first-principle model for a quantum rotor immersed in an interacting

boson gas. By Bogoliubov approximation and transformation, one can interpret the weakly-interacting boson as a macroscopic state, the Bose-Einstein condensate plus a collective excitation, the phonon. The rotor is dressed by phonons, forming a quasiparticle, which is angulon. Next, we introduced a single-excitation ansatz, which is a generalized second-order perturbation theory. We calculate the variational energy, effective rotational constants, and spectral function. In addition to repeating the calculations of prior research, we derived the real-time evolution equations of motion for the single-excitation ansatz, allowing for an easier numerical calculation of rotational spectroscopy.

In Chapter 4, we proposed a coherent state ansatz in the co-rotating frame as means of describing the effective rotational constants effectively and efficiently. It first uses a rotational transformation to transfer to the molecular frame, similar to the Lee-Low-Pines approach. The canonical transformation is used to decouple the impurity. Vice versa it can also be interpreted as a transformation to entangle the impurity and bath. The rotor is thus entangled with the bath, even though it is only partially decoupled due to the non-Abelian $SO(3)$ algebra. Next, we considered a product state ansatz between the angular and bosonic coherent states. For such a product state structure, an effective model can be obtained by tracing out the angular or bosonic state. We are able to optimize the variational parameters in an iterative way. Using this technique, we discovered that the ground state can be described by a product state between an anomalous spin coherent state and a bosonic coherent state. Importantly, this ansatz always predicts a decreased effective rotational constant, consistent with experimental findings. We also studied the spectral function by the real-time evolution of the coherent state ansatz. It shows that the quasiparticles are unstable in the intermediate-density regime and the spectral lines are significantly broadened.

In Chapter 5, we used Fermi's golden rule to examine the rotational spectroscopy for the $L = 0 \to 1$ transition with both the single-excitation ansatz and coherent state ansatz. We took into account the laser perturbation and the equilibrium initial-state, which are neglected in previous research. The coherent state predicts a trivial sharp spectral line, which indicates that the coherent state ansatz is not sufficient for describing excited states. Meanwhile, the single-excitation ansatz predicts an instability regime, where the spectral lines are broadened. The phonon wing, which is observed in the spectral function, cannot be observed in this case, because the equilibrium initial-state has no overlaps with the excited states. This resolves the con-

flict between the theory and experiment of having no phonon wings being observed despite their presence in simple angulon theory.

Outlook

In this thesis, we employed both the single-excitation and the coherent state ansatz. However, both could only explain a part of the experimental results. The coherent state, which is the exact solution in the slowly-rotating limit, works well in describing the ground-state properties, such as the effective rotational constants, but performs badly in describing the excited-state properties, such as rotational spectroscopy. On the contrary, the single-excitation ansatz works well for the excited-state properties, but is insufficient in describing the ground state. Therefore, it is necessary to generalize the ansatz. In Appendix C, we proposed a multimode coherent state ansatz, which further lowers the static energy. Another possible way is considering a single-excitation over a coherent state. This is similar to Ref. [15], but the coherent state should be treated variationally.

What's more, the Bogoliubov approximation in deriving the angulon model restricts us to treat the boson-boson interaction within a mean-field framework, which is only valid when the interaction is weak and the Bogoliubov phonons are stable. With the coherent state method, it is possible to directly deal with the first-principle model, the quantum rotor immersed in the interacting boson gas. In this way, one can expect to gain a deeper insight into the quasiparticle instability regime as well as higher angular momentum sectors.

Appendix A

Notations

A.1 Angular momentum representation of bosonic operators

In this thesis, the Fourier transformation and inverse transformation of bosonic operators is defined as

$$\begin{aligned} \hat{b}^\dagger_{\boldsymbol{k}} &= \int d^3 r \hat{b}^\dagger_{\boldsymbol{r}} e^{i\boldsymbol{k}\cdot\boldsymbol{r}}, \\ \hat{b}^\dagger_{\boldsymbol{r}} &= \int \frac{d^3 k}{(2\pi)^3} \hat{b}^\dagger_{\boldsymbol{k}} e^{-i\boldsymbol{k}\cdot\boldsymbol{r}}. \end{aligned} \tag{A.1}$$

In the Angulon problem, we mainly focus on the angular momentum exchange between rotor and bosons. Hence it is more convenient to work in the angular momentum basis.

$$\begin{aligned} \hat{b}^\dagger_{k\lambda\mu} &= \frac{k}{(2\pi)^{3/2}} \int d\Phi_k d\Theta_k \sin\Theta_k \hat{b}^\dagger_{\boldsymbol{k}} i^{-\lambda} Y_{\lambda\mu}(\Theta_k, \Phi_k), \\ \hat{b}^\dagger_{\boldsymbol{k}} &= \frac{(2\pi)^{3/2}}{k} \sum_{\lambda\mu} \hat{b}^\dagger_{k\lambda\mu} i^{\lambda} Y^*_{\lambda\mu}(\Theta_k, \Phi_k). \end{aligned} \tag{A.2}$$

Here the spherical harmonic, $Y_{\lambda\mu}(\Theta_k, \Phi_k)$, is the eigenfunction of angular momentum operators, $\hat{\boldsymbol{L}}^2$ and $\hat{L}^z$.

The corresponding commutation relation in the momentum basis is given by

$$[\hat{b}_{\boldsymbol{k}}, \hat{b}^\dagger_{\boldsymbol{k}}] = (2\pi)^3 \delta^3(\boldsymbol{k} - \boldsymbol{k}'). \tag{A.3}$$

Then we can derive the commutation relation in the angular momentum basis:

$$\begin{aligned}
&[\hat{b}_{k\lambda\mu}, \hat{b}^\dagger_{k'\lambda'\mu'}] \\
=&\frac{kk'}{(2\pi)^3}\int d\Omega_k \int d\Omega_{k'}(-1)^{-\lambda} i^{-\lambda-\lambda'} Y^*_{\lambda\mu}(\Theta_k,\Phi_k) Y_{\lambda'\mu'}(\Theta_{k'},\Phi_{k'})[\hat{b}_{\boldsymbol{k}}, \hat{b}^\dagger_{\boldsymbol{k}'}] \\
=&(-1)^{-\lambda} i^{-\lambda-\lambda'}\delta(k-k')\int d\Omega_k Y^*_{\lambda\mu}(\Theta_k,\Phi_k) Y_{\lambda'\mu'}(\Theta_k,\Phi_k) \\
=&\delta(k-k')\delta_{\lambda\lambda'}\delta_{\mu\mu'},
\end{aligned} \tag{A.4}$$

where $d\Omega_k \equiv d\Phi_k d\Theta_k \sin\Theta_k$ and $\delta^3(\boldsymbol{k}-\boldsymbol{k}') = \frac{1}{kk'\sin\Theta'_{k'}}\delta(k-k')\delta(\Theta_k - \Theta'_k)\delta(\Phi_k - \Phi'_{k'})$.

A.2 Angular momentum operators

The definition of ladder operators is not unique. One convenient definition for calculations, especially for the anomalous angular momentum, is given by [51]

$$\hat{J}_\pm|j,m,n\rangle = \sqrt{j(j+1)}C^{j,m\pm1}_{j,m;1,\pm1}|j,m\pm1,n\rangle, \tag{A.5}$$

$$\hat{J}'_\pm|j,m,n\rangle = -\sqrt{j(j+1)}C^{j,n\mp1}_{j,n;1,\mp1}|j,m,n\mp1\rangle, \tag{A.6}$$

where $k = 0, \pm1$, and $\sqrt{j(j+1)}C^{j,m\pm1}_{j,m;1,\pm1} = \mp\sqrt{(j\mp m)(j\pm m+1)}/\sqrt{2} = \mp\sqrt{j(j+1)-m(m\pm1)}/\sqrt{2}$. And the (anomalous) angular momentum operators are given by

$$\begin{aligned}
\hat{J}^{(\prime)}_x =&\frac{1}{\sqrt{2}}(\hat{J}^{(\prime)}_- - \hat{J}^{(\prime)}_+), \\
\hat{J}^{(\prime)}_y =&\frac{i}{\sqrt{2}}(\hat{J}^{(\prime)}_- + \hat{J}^{(\prime)}_+), \\
\hat{J}^{(\prime)}_z =&\hat{J}^{(\prime)}_0.
\end{aligned} \tag{A.7}$$

Another more common definition is given by [52]

$$\hat{J}_\pm|j,m,n\rangle = \sqrt{(j\mp m)(j\pm m+1)}|j,m\pm1,n\rangle \tag{A.8}$$

and

$$\begin{aligned} \hat{J}_x =& \frac{1}{2}(\hat{J}_- + \hat{J}_+), \\ \hat{J}_y =& \frac{i}{2}(\hat{J}_- - \hat{J}_+). \end{aligned} \tag{A.9}$$

The two definitions have the same matrix elements for $\hat{J}_{x,y,z}$.

Appendix B

Derivation of the anomalous spin coherent state

Here we will derive the ground state of the single anomalous spin model, whose Hamiltonian is given by

$$\hat{H} = -\boldsymbol{n} \cdot \hat{\boldsymbol{J}}', \tag{B.1}$$

where $\boldsymbol{n} = (\sin\theta\cos\phi, \sin\theta\sin\phi, \cos\theta)$. Next we introduce the anomalous rotation operators:

$$\hat{D}'(\alpha, \beta, \gamma) = e^{-i\alpha\hat{J}'^z} e^{-i\beta\hat{J}'^y} e^{-i\gamma\hat{J}'^z}. \tag{B.2}$$

Unlike the normal rotation operator, the anomalous one indicates left-hand rotation [53, 54]. The Hamiltonian can be diagonalized, given by

$$\hat{H} = -\boldsymbol{n} \cdot \hat{\boldsymbol{J}}' = -\hat{D}'(-\phi, -\theta, 0)\hat{J}'^z\hat{D}'^{\dagger}(-\phi, -\theta, 0). \tag{B.3}$$

Then the corresponding ground state is given by

$$|\psi_0\rangle = \hat{D}'(-\phi, -\theta, 0)|LML\rangle = \sum_n g_n |LMn\rangle, \tag{B.4}$$

where the superposition coefficients are given by $g_n = D'^L_{nL}(-\phi, -\theta, 0)$. Here D'^L_{nm} is the anomalous Wigner D matrix, defined as

$$\begin{aligned} D'^L_{nm}(\alpha, \beta, \gamma) =& \langle LMn|e^{-i\alpha\hat{J}'^z} e^{-i\beta\hat{J}'^y} e^{-i\gamma\hat{J}'^z}|LMm\rangle, \\ =& e^{-i\alpha n - i\gamma m}\langle LMn|e^{-i\beta\hat{J}'^y}|LMm\rangle, \\ =& e^{-i\alpha n - i\gamma m} d'^L_{nm}. \end{aligned} \tag{B.5}$$

The small Wigner d-operator and -matrix are defined as $\hat{d}'(\beta) \equiv e^{-i\beta\hat{J}'^y}$ and $d'^L_{nm} = \langle LMn|e^{-i\beta\hat{J}'^y}|LMm\rangle$.

We follow Schwinger's oscillator method to derive an analytical expression for the anomalous small d matrix [52, 55]. In the model we consider two independent harmonic oscillators, whose creation and annihilation operators are labeled by $\hat{a}_+^{(\dagger)}$ and $\hat{a}_-^{(\dagger)}$, respectively, and they satisfy bosonic commutation relations, $[\hat{a}_\pm, \hat{a}_\pm^\dagger] = 1$. And we consider the particle number basis:

$$|n_+, n_-\rangle = \frac{(a_+^\dagger)^{n_+}(a_-^\dagger)^{n_-}}{\sqrt{n_+!n_-!}}|0,0\rangle. \tag{B.6}$$

Next, we introduce the anomalous angular momentum operator represented by the oscillator operators:

$$\hat{J}'^+ = -\frac{1}{\sqrt{2}}\hat{a}_+^\dagger\hat{a}_-;\ \ \hat{J}'^- = \frac{1}{\sqrt{2}}\hat{a}_-^\dagger\hat{a}_+; \tag{B.7}$$

$$\hat{J}'^z = \frac{1}{2}(\hat{a}_-^\dagger\hat{a}_- - \hat{a}_+^\dagger\hat{a}_+); \tag{B.8}$$

$$J'^x \equiv \frac{1}{\sqrt{2}}(\hat{J}'^- - \hat{J}'^+);\ \ J'^y = \frac{i}{\sqrt{2}}(\hat{J}'^- + \hat{J}'^+). \tag{B.9}$$

It is easy to check that they satisfy the anomalous commutation relations Eq. (4.3). If we make a shift $n_+ = L - n;\ n_- = L + n$, the particle number basis can be written in the anomalous angular momentum basis:

$$|n_+, n_-\rangle \to |LMn\rangle = \frac{(a_+^\dagger)^{L-n}(a_-^\dagger)^{L+n}}{\sqrt{(L-n)!(L+n)!}}|0\rangle, \tag{B.10}$$

where the second quantum number M is irrelevant. The state satisfies

$$\hat{J}'^z|LMn\rangle = n|LMn\rangle, \tag{B.11}$$

$$\hat{\boldsymbol{J}}'^2|LMn\rangle = L(L+1)|LMn\rangle. \tag{B.12}$$

$$\hat{J}'^+|LMn\rangle = -\frac{1}{\sqrt{2}}\sqrt{(L+n)(L-n+1)}|LM(n-1)\rangle \tag{B.13}$$

$$\hat{J}'^-|LMn\rangle = \frac{1}{\sqrt{2}}\sqrt{(L-n)(L+n+1)}|LM(n+1)\rangle \tag{B.14}$$

Now, we can use the above representation to calculate the corresponding anomalous small d matrix:

$$\begin{aligned}
&e^{-i\beta\hat{J}'^{y}}|LMm\rangle \\
=&\frac{[\hat{d}'(\beta)\hat{a}_{+}^{\dagger}\hat{d}'^{\dagger}(\beta)]^{L-m}[\hat{d}'(\beta)\hat{a}_{-}^{\dagger}\hat{d}'^{\dagger}(\beta)]^{L+m}}{\sqrt{(L-m)!(L+m)!}}\hat{d}(\beta)|0\rangle \\
=&\frac{[\cos\frac{\beta}{2}\hat{a}_{+}^{\dagger}+\sin\frac{\beta}{2}\hat{a}_{-}^{\dagger}]^{L-m}[\cos\frac{\beta}{2}\hat{a}_{-}^{\dagger}-\sin\frac{\beta}{2}\hat{a}_{+}^{\dagger}]^{L+m}}{\sqrt{(L-m)!(L+m)!}}|0\rangle \\
=&\sum_{m'}|LMm'\rangle d'^{(L)}_{m'm}(\beta)
\end{aligned} \tag{B.15}$$

where $\hat{d}'(\theta)\hat{a}_{\pm}^{\dagger}\hat{d}'^{\dagger}(\theta)=\cos\frac{\theta}{2}a_{\pm}^{\dagger}\pm\sin\frac{\theta}{2}a_{\mp}^{\dagger}$ and

$$\begin{aligned}
d'^{(L)}_{m'm}(\beta)=&\sum_{k}(-1)^{k+m+m'}\frac{\sqrt{(j-m)!(j+m)!(j+m')!(j-m')!}}{(j-m-k)!k!(j-m'-k)!(k+m+m')!} \\
&\times(\cos\frac{\beta}{2})^{2j-2k-m-m'}(\sin\frac{\beta}{2})^{2k+m+m'}.
\end{aligned} \tag{B.16}$$

We can next calculate the superposition coefficients for the anomalous spin coherent state, which is a special case of the Wigner d-operator with $m=L$, given by:

$$\begin{aligned}
&\hat{D}'(-\phi,-\theta)|LML\rangle \\
=&e^{i\phi\hat{J}'^{z}}\frac{[\hat{d}'(-\theta)a_{-}^{\dagger}\hat{d}'^{\dagger}(-\theta)]^{2L}}{\sqrt{(2L)!}}|0\rangle \\
=&\sum_{n}\binom{2L}{L+n}^{1/2}(\cos\frac{\theta}{2})^{L+n}(\sin\frac{\theta}{2})^{L-n}e^{i\phi n}|LMn\rangle.
\end{aligned} \tag{B.17}$$

Without loss of generality, we can introduce a global phase and obtain the superposition coefficients:

$$g_n=\binom{2L}{L+n}^{1/2}(\cos\frac{\theta}{2})^{L+n}(\sin\frac{\theta}{2})^{L-n}e^{-i\phi(L-n)}. \tag{B.18}$$

Then, one can calculate the expectation values of the anomalous angular

momentum:

$$
\begin{aligned}
J'^x =& \langle \hat{J}'^x \rangle \\
=& \langle LML | e^{-i\theta \hat{J}'^y} e^{-i\phi \hat{J}'^z} \hat{J}'^x e^{i\phi \hat{J}'^z} e^{i\theta \hat{J}'^y} | LML \rangle \\
=& \langle LML | e^{-i\theta \hat{J}'^y} (\cos\phi \hat{J}'^x + \sin\phi \hat{J}'^y) e^{i\theta \hat{J}'^y} | LML \rangle \\
=& \langle LML | (\cos\phi (\cos\phi \hat{J}'^x + \sin\phi \hat{J}'^z) + \sin\phi \hat{J}'_y) | LML \rangle \\
=& L \sin\theta \cos\phi,
\end{aligned}
\tag{B.19}
$$

$$
\begin{aligned}
J'^y =& \langle \hat{J}'^y \rangle \\
=& \langle LML | e^{-i\theta \hat{J}'^y} e^{-i\phi \hat{J}'^z} \hat{J}'^y e^{i\phi \hat{J}'^z} e^{i\theta \hat{J}'^y} | LML \rangle \\
=& \langle LML | e^{-i\theta \hat{J}'^y} (\cos\phi \hat{J}'^y - \sin\phi \hat{J}'^x) e^{i\theta \hat{J}'^y} | LML \rangle \\
=& \sin\theta \sin\phi \langle LML | \hat{J}'_z | LML \rangle \\
=& L \sin\theta \sin\phi,
\end{aligned}
\tag{B.20}
$$

$$
\begin{aligned}
J'^z =& \langle \hat{J}'^z \rangle \\
=& \langle LML | e^{-i\theta \hat{J}'^y} e^{-i\phi \hat{J}'^z} \hat{J}'^z e^{i\phi \hat{J}'^z} e^{i\theta \hat{J}'^y} | LML \rangle \\
=& \langle LML | e^{-i\theta \hat{J}'^y} \hat{J}'^z e^{i\theta \hat{J}'^y} | LML \rangle \\
=& \langle LML | (\cos\theta \hat{J}'^z - \sin\theta \hat{J}'^x) | LML \rangle \\
=& L \cos\theta.
\end{aligned}
\tag{B.21}
$$

Appendix C

Multimode coherent state ansatz

The coherent state ansatz Eq. (4.8) works well only for low angular momentum sectors since the product state structure does not include enough entanglement between the angular and the bosonic state. A straightforward way to generalize is letting each mode of angular state $|LMn\rangle$ accompanied by a singlemode coherent state $|C_n\rangle = \hat{U}_n|0\rangle = e^{\hat{B}^\dagger \sigma^z \Delta_n}|0\rangle$. Hence, we propose a multimode coherent state ansatz, which is given by

$$|\psi\rangle = \sum_n g_n |LMn\rangle \otimes e^{\hat{B}^\dagger \sigma^z \Delta_n}|0\rangle = \sum_n g_n |n\rangle \otimes \hat{U}_n|0\rangle. \tag{C.1}$$

Here we use the Nambu basis for convenience: $\hat{B} = (\hat{b}, \hat{b}^\dagger)^T$, $\Delta = (\beta, \beta^*)^T$. This ansatz is similar to the so-called Silbey-Harris ansatz [56–58] in studying the spin-boson model.

Imaginary-time evolution

We first consider a general Hamiltonian and derive the equation of motion for imaginary-time evolution to optimize the variational parameters for the ground state, starting from

$$\partial_\tau |\psi\rangle = -(\hat{H} - E)|\psi\rangle. \tag{C.2}$$

The left-hand side can be expanded as

$$\begin{aligned} \partial_\tau |\psi\rangle = &\sum_n \hat{U}_n (\partial_\tau g_n)|0\rangle|n\rangle \\ &+ \sum_n g_n \hat{U}_n (\frac{1}{2}\Delta_n^\dagger \sigma^z \partial_\tau \Delta_n + \hat{B}^\dagger \sigma^z \partial_\tau \Delta_n)|0\rangle|n\rangle. \end{aligned} \tag{C.3}$$

One can obtain the equation of motion for $\partial_\tau \beta_{n,k}$ by projecting out the one phonon state $\langle n|\langle 0|\hat{b}_k$:

$$\begin{aligned}
&\langle n|\langle 0|\hat{b}_k \hat{U}_n^\dagger \partial_t |\psi\rangle \\
=&\partial_\tau g_n \langle 0|\hat{b}_k|0\rangle + g_n \frac{1}{2}\Delta_{b,n}^\dagger \sigma^z \partial_\tau \Delta_n \langle 0|\hat{b}_k|0\rangle + g_n \langle 0|\hat{b}_k \hat{B}^\dagger \sigma^z \partial_\tau \Delta_n|0\rangle \\
=&g_n \partial_\tau \beta_{n,k}.
\end{aligned} \tag{C.4}$$

Next, we consider the right hand side. The Hamiltonian can be split into diagonal and off-diagonal term for the angular state, $\hat{H} = \hat{H}^d + \hat{H}^o$. One can trace out the angular state, such that $\hat{H}_n^d = \langle n|\hat{H}^d|n\rangle$ and $\hat{H}_{nm}^o = \langle n|\hat{H}^o|m\rangle$. Then the projection can be written as

$$\begin{aligned}
&-\langle n|\langle 0|\hat{b}_k \hat{U}_n^\dagger (\hat{H} - E)|\psi\rangle \\
=&-\langle n|\langle 0|\hat{b}_k \hat{U}_n^\dagger \hat{H}^d|\psi\rangle - \langle n|\langle 0|\hat{b}_k \hat{U}_n^\dagger \hat{H}^o|\psi\rangle + E\langle n|\langle 0|\hat{b}_k \hat{U}_n^\dagger)|\psi\rangle.
\end{aligned} \tag{C.5}$$

The third term is given by

$$\langle n|\langle 0|\hat{b}_k \hat{U}_n^\dagger|\psi\rangle = g_n \langle 0|\hat{b}_k|0\rangle = 0. \tag{C.6}$$

The diagonal term is given by

$$\begin{aligned}
&\langle n|\langle 0|\hat{b}_k \hat{U}_n^\dagger \hat{H}^d|\psi\rangle \\
=&g_n \langle 0|\hat{b}_k \hat{U}_n^\dagger \hat{H}_n^d \hat{U}_n|0\rangle \\
=&g_n \langle 0|\hat{b}_k \hat{B}^\dagger h_n^d|0\rangle \\
=&g_n \eta_{n,k},
\end{aligned} \tag{C.7}$$

where the diagonal Hamiltonian can be approximated as a mean-field energy plus one-excitation term $\hat{H}_n^d \approx E_n^d + \delta \hat{B}_n^\dagger h_n^d$.

The off-diagonal term is given by

$$\begin{aligned}
&\langle n|\langle 0|\hat{b}_k \hat{U}_n^\dagger \hat{H}^o|\psi\rangle \\
=&\sum_m g_m \langle 0|\hat{b}_k \hat{U}_n^\dagger \hat{H}_{nm}^o \hat{U}_m|0\rangle \\
=&\sum_m g_m [\langle 0|\hat{U}_n^\dagger \hat{H}_{nm}^o \hat{b}_k \hat{U}_m|0\rangle + \langle 0|\hat{U}_n^\dagger [\hat{b}_k, \hat{H}_{nm}^o] \hat{U}_m|0\rangle - \beta_{n,k}\langle 0|\hat{U}_n^\dagger \hat{H}_{nm}^o \hat{U}_m|0\rangle] \\
=&\sum_m g_m [(\beta_{m,k} - \beta_{n,k})\langle 0|\hat{U}_n^\dagger \hat{H}_{nm}^o \hat{U}_m|0\rangle + \langle 0|\hat{U}_n^\dagger [\hat{b}_k, \hat{H}_{nm}^o] \hat{U}_m|0\rangle]
\end{aligned} \tag{C.8}$$

Therefore, the equation of motion for β_n can be written as

$$g_n\partial_\tau\beta_{n,k} = -g_n\eta_{n,k} - \sum_m g_m[(\beta_{m,k}-\beta_{n,k})\langle 0|\hat{U}_n^\dagger\hat{H}_{nm}^o\hat{U}_m|0\rangle + \langle 0|\hat{U}_n^\dagger[\hat{b}_k,\hat{H}_{nm}^o]\hat{U}_m|0\rangle]. \tag{C.9}$$

Diagonalization of the angular state

We next consider the angular state using a diagonalization method. The variational energy can be expanded in a matrix form:

$$\begin{aligned}
&E = \langle\psi|\hat{H}|\psi\rangle = \langle\psi|\hat{H}^d + \hat{H}^o|\psi\rangle \\
=&\sum_n |g_n|^2 E_n^d + \sum_{nm} g_n^* g_m \langle C_n|\hat{H}_{nm}^o(\hat{b}^\dagger,\hat{b})|C_m\rangle \\
=&\sum_n |g_n|^2 E_n^d + \sum_{nm} g_n^* g_m H_{nm}^o(\beta_n^*,\beta_m)\langle C_n|C_m\rangle \\
=&\sum_n |g_n|^2 E_n^d + \sum_{nm} g_n^* E_{nm}^o g_m \\
=&\begin{pmatrix} g_1^* & g_2^* & \cdots & g_N^* \end{pmatrix}
\begin{pmatrix} E_1^d+E_{11}^o & E_{12}^o & \cdots & \\ E_{21}^o & E_2^d+E_{22}^o & \ddots & \\ \vdots & \ddots & \ddots & \\ & & & E_N^d+E_{NN}^o \end{pmatrix}
\begin{pmatrix} g_1 \\ g_2 \\ \vdots \\ g_N \end{pmatrix}
\end{aligned} \tag{C.10}$$

where $\hat{H}_{nm}^o$ is normal ordered about $\hat{b}$ and $H_{nm}^o = \hat{H}_{nm}^o(\hat{b}^{(\dagger)} \to \beta^{(*)})$, and $E_{nm}^o = H_{nm}^o\langle C_n|C_m\rangle$. The inner product between the two coherent states reads

$$P_{nm} = \langle C_n|C_m\rangle = e^{-\frac{1}{2}\beta_n^\dagger\beta_n + \beta_n^\dagger\beta_m - \frac{1}{2}\beta_m^\dagger\beta_m}. \tag{C.11}$$

Then we can minimize the energy by diagonalizing the energy matrix.

Angulon

Next, we go back to the angulon problem, which can be split into two parts:

$$\hat{H} = \hat{H}^d + \hat{H}^o \tag{C.12}$$

where the diagonal term reads

$$\begin{aligned}\hat{H}^d =& B\hat{\boldsymbol{J}'}^2 + \sum_{k\lambda} V_\lambda(k)(\hat{b}^\dagger_{k\lambda 0} + \hat{b}_{k\lambda 0}) + \sum_{k\lambda\mu} W_{k\lambda}\hat{b}^\dagger_{k\lambda\mu}\hat{b}_{k\lambda\mu} \\ &+ B\sum_\alpha \sum_{k\lambda\mu\nu}\sum_{ql\rho\sigma} \sigma^{\lambda,\alpha}_{\mu\nu}\sigma^{l,\alpha}_{\rho\sigma}\hat{b}^\dagger_{k\lambda\mu}\hat{b}^\dagger_{ql\rho}\hat{b}_{ql\sigma}\hat{b}_{k\lambda\nu},\end{aligned} \tag{C.13}$$

and the off-diagonal term reads

$$\hat{H}^o = -2B\sum_\alpha \sum_{k\lambda\mu\nu} \hat{J}'^{,\alpha}\hat{b}^\dagger_{k\lambda\mu}\sigma^{\lambda,\alpha}_{\mu\nu}\hat{b}_{k\lambda\nu}. \tag{C.14}$$

The variational energy is given by

$$\begin{aligned}E =& \langle\psi|\hat{H}|\psi\rangle \\ =& \langle\psi|\hat{H}^d|\psi\rangle + \langle\psi|\hat{H}^o|\psi\rangle \\ =& \sum_n |g_n|^2 E^d_n + \sum_{nm} g^*_n g_m \langle C_n|\hat{H}^o_{nm}|C_m\rangle,\end{aligned} \tag{C.15}$$

where the diagonal part reads

$$\begin{aligned}E^d_n =& BL(L+1) + \sum_{k\lambda} V_\lambda(k)(\beta^*_{n,k\lambda 0} + \beta_{n,k\lambda 0}) \\ &+ \sum_{k\lambda\mu} W_{k\lambda}\beta^*_{n,k\lambda\mu}\beta_{n,k\lambda\mu} + B\sum_\alpha \Lambda^\alpha_n\Lambda^\alpha_n,\end{aligned} \tag{C.16}$$

and the off-diagonal part reads

$$\begin{aligned}&\langle C_n|\hat{H}^o_{nm}|C_m\rangle \\ =& -2B\sum_\alpha\sum_{k\lambda\mu\nu} J'^{,\alpha}_{nm}\langle C_n|\hat{b}^\dagger_{k\lambda\mu}\sigma^{\lambda,\alpha}_{\mu\nu}\hat{b}_{k\lambda\nu}|C_m\rangle \\ =& -2B\sum_\alpha\sum_{k\lambda\mu\nu} J'^{,\alpha}_{nm}\beta^*_{n,k\lambda\mu}\sigma^{\lambda,\alpha}_{\mu\nu}\beta_{m,k\lambda\nu}\langle C_n|C_m\rangle \\ =& -2B\sum_\alpha J'^{,\alpha}_{nm}\Lambda^\alpha_{nm}P_{nm}.\end{aligned} \tag{C.17}$$

As discussed above, the diagonal part can be approximated as a mean-field energy plus a one-excitation fluctuation:

$$\hat{H}^d_n \approx E^d_n + \delta B^\dagger_n h_n = E^d_n + (\sum_{k\lambda\mu}\delta\hat{b}^\dagger_{n,k\lambda\mu}\eta_{k\lambda\mu} + h.c.). \tag{C.18}$$

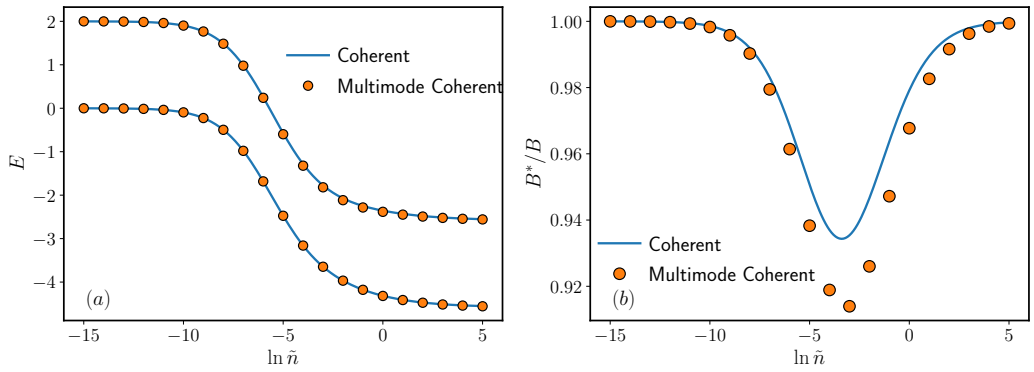

Figure C.1: (a) The energy for $L = 0, 1$ and (b) the effective rotational constant obtained by the coherent state and multimode coherent state ansatz.

Here the fluctuation is given by

$$\eta_{n,k\lambda\mu} = V_\lambda(k)\delta_{\mu,0} + W_{k\lambda}\beta_{n,k\lambda\mu} + 2B\sum_\alpha\sum_\nu \sigma^{\lambda,\alpha}_{\mu\nu}\beta_{n,k\lambda\nu}\Lambda^\alpha_n. \tag{C.19}$$

One can calculate the building-blocks for the off-diagonal term:

$$\langle C_n|\hat{H}^o_{nm}|C_m\rangle = -2B\sum_\alpha J'^{,\alpha}_{nm}\Lambda^\alpha_{nm}P_{nm}, \tag{C.20}$$

and

$$\langle C_n|[\hat{b}_{k\lambda\mu}, \hat{H}^o_{nm}]|C_m\rangle = -2B\sum_\alpha\sum_\nu J'^{,\alpha}_{nm}\sigma^{\lambda,\alpha}_{\mu\nu}\beta_{m,k\lambda\nu}P_{nm}. \tag{C.21}$$

Then we conclude the equation of motion:

$$\begin{aligned}\partial_\tau\beta_{n,k\lambda\mu} &= -\eta_{n,k\lambda\mu} \\ &+ \frac{2B}{g_n}\sum_m g_m P_{nm}\sum_\alpha J'^{,\alpha}_{nm}[\Lambda^\alpha_{nm}(\beta_{m,k\lambda\mu} - \beta_{n,k\lambda\mu}) + \sum_\nu \sigma^{\lambda,\alpha}_{\mu\nu}\beta_{m,k\lambda\nu}].\end{aligned} \tag{C.22}$$

In Fig. C.1, we compare the static energy and the effective rotational constant obtained by the coherent state and multimode coherent state ansatz. And in Fig. C.2, we show the displacement vector for the multimode coherent state. For $L = 0$, the two ansatzes coincide with each other thus predict the same energy. For $L = 1$, the entanglement between different modes plays a role, and the multimode coherent state compresses the static energy and significantly lowers the effective rotational constant.

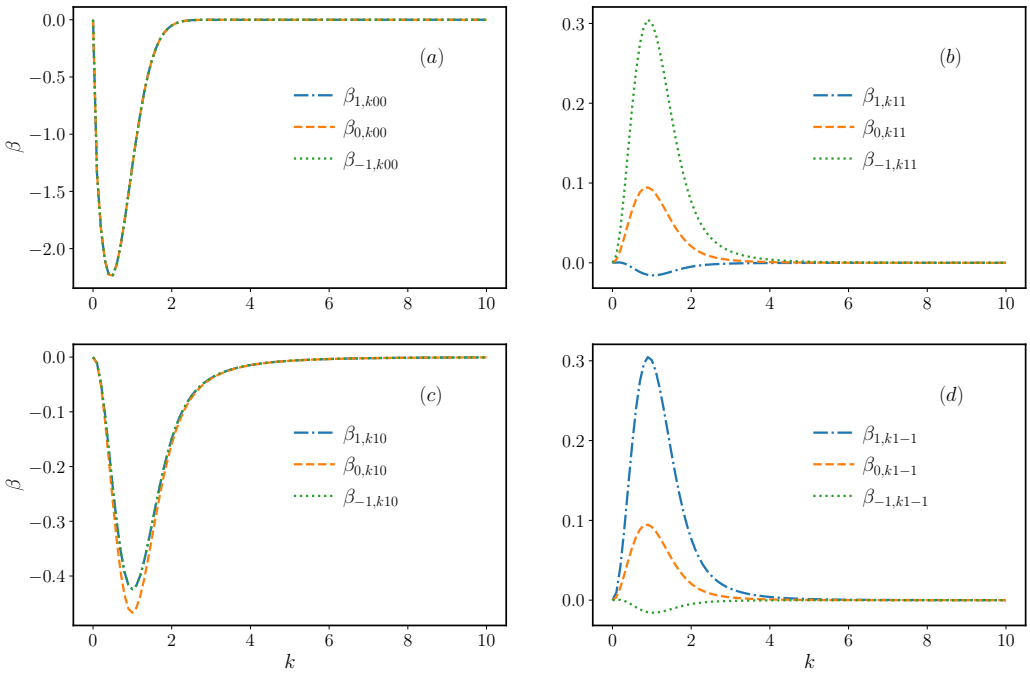

Figure C.2: The multimode displacement vector $\beta_{n,k\lambda\mu}$ for $L = 1$ and $\ln \tilde{n} = -3$.

Bibliography

[1] J. P. Toennies and A. F. Vilesov, "Superfluid helium droplets: A uniquely cold nanomatrix for molecules and molecular complexes," Angewandte Chemie International Edition **43**, 2622–2648 (2004).

[2] S. Yang and A. M. Ellis, "Helium droplets: a chemistry perspective," Chem. Soc. Rev. **42**, 472–484 (2013).

[3] M. Hartmann, F. Mielke, J. P. Toennies, A. F. Vilesov, and G. Benedek, "Direct spectroscopic observation of elementary excitations in superfluid he droplets," Phys. Rev. Lett. **76**, 4560–4563 (1996).

[4] S. Grebenev, J. P. Toennies, and A. F. Vilesov, "Superfluidity within a small helium-4 cluster: The microscopic andronikashvili experiment," Science **279**, 2083–2086 (1998).

[5] F. Stienkemeier and K. K. Lehmann, "Spectroscopy and dynamics in helium nanodroplets," Journal of Physics B: Atomic, Molecular and Optical Physics **39**, R127–R166 (2006).

[6] C. Callegari, K. K. Lehmann, R. Schmied, and G. Scoles, "Helium nanodroplet isolation rovibrational spectroscopy: Methods and recent results," J. Chem. Phys. **115**, 10090–10110 (2001).

[7] A. M. Morrison, P. L. Raston, and G. E. Douberly, "Rotational dynamics of the methyl radical in superfluid 4he nanodroplets," The Journal of Physical Chemistry A **117**, 11640–11647 (2013), pMID: 23214951.

[8] L. D. Landau, "Über Die Bewegung der Elektronen in Kristallgitter," Phys. Z. Sowjetunion **3**, 644–645 (1933).

[9] S. I. Pekar, Journ. of Phys. USSR **10**, 341 (1946).

[10] H. Fröhlich, "Electrons in lattice fields," Advances in Physics **3**, 325–361 (1954).

[11] R. E. Zillich, Y. Kwon, and K. B. Whaley, "Roton-rotation coupling of acetylene in ^{4}He," Phys. Rev. Lett. **93**, 250401 (2004).

[12] R. E. Zillich and K. B. Whaley, "Quantum rotation of hcn and dcn in ^{4}He," Phys. Rev. B **69**, 104517 (2004).

[13] R. E. Zillich and K. B. Whaley, "Rotational spectra of methane and deuterated methane in helium," The Journal of Chemical Physics **132**, 174501 (2010).

[14] R. Schmidt and M. Lemeshko, "Rotation of quantum impurities in the presence of a many-body environment," Phys. Rev. Lett. **114**, 203001 (2015).

[15] R. Schmidt and M. Lemeshko, "Deformation of a quantum many-particle system by a rotating impurity," Phys. Rev. X **6**, 011012 (2016).

[16] M. Lemeshko and R. Schmidt, "Molecular impurities interacting with a many-particle environment: from helium droplets to ultracold gases," arXiv:1703.06753 (2017).

[17] M. Lemeshko, "Quasiparticle approach to molecules interacting with quantum solvents," Phys. Rev. Lett. **118**, 095301 (2017).

[18] I. N. Cherepanov and M. Lemeshko, "Fingerprints of angulon instabilities in the spectra of matrix-isolated molecules," Phys. Rev. Materials **1**, 035602 (2017).

[19] I. Bloch, J. Dalibard, and W. Zwerger, "Many-body physics with ultracold gases," Rev. Mod. Phys. **80**, 885–964 (2008).

[20] C. Kohstall, M. Zaccanti, M. Jag, A. Trenkwalder, P. Massignan, G. M. Bruun, F. Schreck, and R. Grimm, "Metastability and coherence of repulsive polarons in a strongly interacting fermi mixture," Nature **485**, 615–618 (2012).

[21] M.-G. Hu, M. J. Van de Graaff, D. Kedar, J. P. Corson, E. A. Cornell, and D. S. Jin, "Bose polarons in the strongly interacting regime," Phys. Rev. Lett. **117**, 055301 (2016).

[22] N. B. Jørgensen, L. Wacker, K. T. Skalmstang, M. M. Parish, J. Levinsen, R. S. Christensen, G. M. Bruun, and J. J. Arlt, "Observation of attractive and repulsive polarons in a bose-einstein condensate," Phys. Rev. Lett. **117**, 055302 (2016).

[23] A. Schirotzek, C.-H. Wu, A. Sommer, and M. W. Zwierlein, "Observation of fermi polarons in a tunable fermi liquid of ultracold atoms," Phys. Rev. Lett. **102**, 230402 (2009).

[24] T. Dieterle, M. Berngruber, C. Hölzl, R. Löw, K. Jachymski, T. Pfau, and F. Meinert, "Transport of a single cold ion immersed in a bose-einstein condensate," Phys. Rev. Lett. **126**, 033401 (2021).

[25] P. Massignan, M. Zaccanti, and G. M. Bruun, "Polarons, dressed molecules and itinerant ferromagnetism in ultracold fermi gases," Reports on Progress in Physics **77**, 034401 (2014).

[26] M. Bruderer, A. Klein, S. R. Clark, and D. Jaksch, "Polaron physics in optical lattices," Phys. Rev. A **76**, 011605 (2007).

[27] M. Bruderer, A. Klein, S. R. Clark, and D. Jaksch, "Transport of strong-coupling polarons in optical lattices," New Journal of Physics **10**, 033015 (2008).

[28] F. Grusdt, A. Shashi, D. Abanin, and E. Demler, "Bloch oscillations of bosonic lattice polarons," Phys. Rev. A **90**, 063610 (2014).

[29] M. Sun, H. Zhai, and X. Cui, "Visualizing the efimov correlation in bose polarons," Phys. Rev. Lett. **119**, 013401 (2017).

[30] P. Naidon and S. Endo, "Efimov physics: a review," Reports on Progress in Physics **80**, 056001 (2017).

[31] A. Guidini, G. Bertaina, D. E. Galli, and P. Pieri, "Condensed phase of bose-fermi mixtures with a pairing interaction," Phys. Rev. A **91**, 023603 (2015).

[32] G. Ness, C. Shkedrov, Y. Florshaim, O. K. Diessel, J. von Milczewski, R. Schmidt, and Y. Sagi, "Observation of a smooth polaron-molecule transition in a degenerate fermi gas," Phys. Rev. X **10**, 041019 (2020).

[33] J. T. Devreese, "Fröhlich polarons. lecture course including detailed theoretical derivations," arXiv:1012.4576 [cond-mat] (2015).

[34] Z. Li, *graduate teaching books: Solid State Theory* (Higher Education Press Pub., Beijing, 1991).

[35] F. Chevy, "Bose polarons that strongly interact," Physics **9** (2016).

[36] F. Chevy, "Universal phase diagram of a strongly interacting fermi gas with unbalanced spin populations," Phys. Rev. A **74**, 063628 (2006).

[37] R. B. Laughlin, "Anomalous quantum hall effect: An incompressible quantum fluid with fractionally charged excitations," Phys. Rev. Lett. **50**, 1395–1398 (1983).

[38] T. D. Lee, F. E. Low, and D. Pines, "The motion of slow electrons in a polar crystal," Phys. Rev. **90**, 297–302 (1953).

[39] P. O. Scherer and S. F. Fischer, *Theoretical molecular biophysics* (Springer, 2010).

[40] J. P. Lowe and K. Peterson, *Quantum chemistry* (Elsevier, 2011).

[41] Y. Shchadilova, "A new angle on quantum impurities," Physics **10**, 20 (2017).

[42] L. D. Landau and E. M. Lifshitz, *Quantum mechanics: non-relativistic theory*, Vol. 3 (Elsevier, 2013).

[43] L. Pitaevskii and S. Stringari, *Bose-Einstein condensation and superfluidity*, Vol. 164 (Oxford University Press, 2016).

[44] N. N. Bogolyubov, "On the theory of superfluidity," J.Phys.(USSR) **11**, 23–32 (1947).

[45] B. Midya, M. Tomza, R. Schmidt, and M. Lemeshko, "Rotation of cold molecular ions inside a bose-einstein condensate," Phys. Rev. A **94**, 041601 (2016).

[46] E. Yakaboylu and M. Lemeshko, "Anomalous screening of quantum impurities by a neutral environment," Phys. Rev. Lett. **118**, 085302 (2017).

[47] T. Shi, E. Demler, and J. Ignacio Cirac, "Variational study of fermionic and bosonic systems with non-gaussian states: Theory and applications," Annals of Physics **390**, 245–302 (2018).

[48] Y. Wang, I. Esterlis, T. Shi, J. I. Cirac, and E. Demler, "Zero-temperature phases of the two-dimensional hubbard-holstein model: A non-gaussian exact diagonalization study," Phys. Rev. Research **2**, 043258 (2020).

[49] P. W. Anderson, "Infrared catastrophe in fermi gases with local scattering potentials," Phys. Rev. Lett. **18**, 1049–1051 (1967).

[50] M. Knap, A. Shashi, Y. Nishida, A. Imambekov, D. A. Abanin, and E. Demler, "Time-dependent impurity in ultracold fermions: Orthogonality catastrophe and beyond," Phys. Rev. X **2**, 041020 (2012).

[51] D. A. Varshalovich, A. N. Moskalev, and V. K. Khersonskii, *Quantum Theory of Angular Momentum* (WORLD SCIENTIFIC, 1988).

[52] J. Sakurai and J. Napolitano, "Modern quantum mechanics, 2: nd edition," Person New International edition (2011).

[53] M. A. Morrison and G. A. Parker, "A guide to rotations in quantum mechanics," Aust. J. Phys. **40**, 465–498 (1987).

[54] P. P. Man, "Wigner active and passive rotation matrices applied to nmr tensor," Concepts in Magnetic Resonance Part A **45A**, e21385 (2017).

[55] J. Schwinger, L. Biedenharn, and H. Van Dam, "Quantum theory of angular momentum," (1965).

[56] R. Silbey and R. A. Harris, "Variational calculation of the dynamics of a two level system interacting with a bath," The Journal of Chemical Physics **80**, 2615–2617 (1984).

[57] R. A. Harris and R. Silbey, "Variational calculation of the tunneling system interacting with a heat bath. ii. dynamics of an asymmetric tunneling system," The Journal of Chemical Physics **83**, 1069–1074 (1985).

[58] S. Bera, S. Florens, H. U. Baranger, N. Roch, A. Nazir, and A. W. Chin, "Stabilizing spin coherence through environmental entanglement

in strongly dissipative quantum systems," Phys. Rev. B **89**, 121108 (2014).

Acknowledgements

The last two and a half years have been very challenging and dramatic for me, but I've had the good fortune of meeting many fantastic people and receiving a lot of advice.

I would first like to express my gratitude to my supervisor Prof. Richard Schmidt, who began hosting me when I just become a master's student. He not only taught me a lot in physics, but he also gave me advice about my career and life. He is a person who exudes passion and energy, and he never fails to encourage me when I am feeling stuck in my study. In addition, I am delighted to have spent two years at MPQ's quantum matter theory group. I'd like to thank everyone in the group who lends a helping hand whenever I'm in need. We not only shared much office time and also some wine time. And I want to thank Prof. Ignacio Cirac, my TMP program mentor and this thesis's second referee. It is a pleasure for me to be acquainted with him. Even though we only talks a few times, I am impressed by his sharp prospects in research fields. I also want to thank Dr. Enderalp Yakaboylu and Prof. Mikhail Lemeshko for the useful discussion.

I would especially like to thank Prof. Tao Shi from ITP, CAS. He supervised my bachelor thesis in 2019, and it was thanks to him that I was able to join Richard's group. Even after I left, he treats me as his student. We discuss a lot about how to generalize this thesis, such as going beyond the Bogoliubov approximation and the multi-mode coherent states. I am impressed by his humor in life and his rigorous attitude to research.

Next, I want to thank my friends. The first is our little Chinese community at MPQ, which has provided me with irreplaceable help. I had numerous difficulties when I just arrived as a foreigner. My life would be much more difficult without their help. Giuliano Giudici is the second. He lends me helps without expecting anything in return. I really appreciate it.

Last but not least, I would like to express my gratitude to my family. My

parents, particularly my mother, have always encouraged me to pursue my goals and have never interfered with my decisions. My girlfriend Yahui Li accompany me and is very tolerant of my flaws.

The last two years are also difficult for the world. Hope the pandemic will be over soon and our planet will be able to move forward.

Declaration of Authorship

I hereby declare that this thesis has been composed by myself and is based entirely on my work unless where clearly stated otherwise.

Zhongda Zeng

Signature, city, date